

Review

The Spatial and Spectral Resolution of ASTER Infrared Image Data: A Paradigm Shift in Volcanological Remote Sensing

Michael S. Ramsey *  and Ian T.W. Flynn

Department of Geology and Environmental Science, University of Pittsburgh, 4107 O'Hara Street, Pittsburgh, PA 15260-3332, USA; ITF2@pitt.edu

* Correspondence: mramsey@pitt.edu

Received: 26 December 2019; Accepted: 12 February 2020; Published: 23 February 2020



Abstract: During the past two decades, the Advanced Spaceborne Thermal Emission and Reflection Radiometer (ASTER) instrument on the Terra satellite has acquired nearly 320,000 scenes of the world's volcanoes. This is ~10% of the data in the global ASTER archive. Many of these scenes captured volcanic activity at never before seen spatial and spectral scales, particularly in the thermal infrared (TIR) region. Despite this large archive of data, the temporal resolution of ASTER is simply not adequate to understand ongoing eruptions and assess the hazards to local populations in near real time. However, programs designed to integrate ASTER into a volcanic data sensor web have greatly improved the cadence of the data (in some cases, to as many as 3 scenes in 48 h). This frequency can inform our understanding of what is possible with future systems collecting similar data on the daily or hourly time scales. Here, we present the history of ASTER's contributions to volcanology, highlighting unique aspects of the instrument and its data. The ASTER archive was mined to provide statistics including the number of observations with volcanic activity, its type, and the average cloud cover. These were noted for more than 2000 scenes over periods of 1, 5 and 20 years.

Keywords: ASTER; thermal infrared data; volcanic processes; image archive; future concepts

1. Introduction

1.1. ASTER Instrument and History

The Advanced Spaceborne Thermal Emission and Reflection Radiometer (ASTER) instrument was launched on the NASA Terra satellite on 18 December 1999. Prior to the instrument beginning its operational phase on 4 March 2000, ASTER acquired several images including the first thermal infrared (TIR) image on 6 February (Figure 1). That image was of Erta Ale volcano (Ethiopia), and initiated a long association of ASTER data with volcanological observations. ASTER was developed and built in Japan under the Japanese Ministry of Economy, Trade and Industry (METI), and is one of five Earth observing instruments on Terra. The combined science team of Japanese and United States investigators has changed over the years, however always maintaining a strong volcanological component [1,2]. During the past two decades, the data from ASTER have been applied to numerous questions and scales of surface processes, most notably for volcanic activity, e.g., [3–6].

ASTER was designed to observe the surface at multiple spatial and spectral resolutions as well as from different viewing geometries. It is actually a suite of three instruments with independent bore-sighted telescopes, originally having 14 spectral channels in the visible/near-infrared (VNIR), the shortwave infrared (SWIR), and the thermal infrared (TIR) regions [7]. The VNIR instrument (0.52–0.86 μm) has three spectral channels at a spatial resolution of 15 m/pixel paired with one channel

oriented in a backward look direction for the creation of digital elevation models (DEMs). The SWIR instrument (1.6–2.43 μm) unfortunately failed in 2008, but originally had six channels at a spatial resolution of 30 m/pixel. Finally, and perhaps most important for many aspects of volcanological remote sensing, the TIR instrument (8.13–11.65 μm) has five channels at a spatial resolution of 90 m/pixel. During the lifetime of the mission, ASTER has acquired over 3.5 million individual scenes—approximately 22% of which were collected at night. Here, we describe the two-decade history of ASTER, specific programs to improve the observational frequency of volcanoes, and present examples of those data.

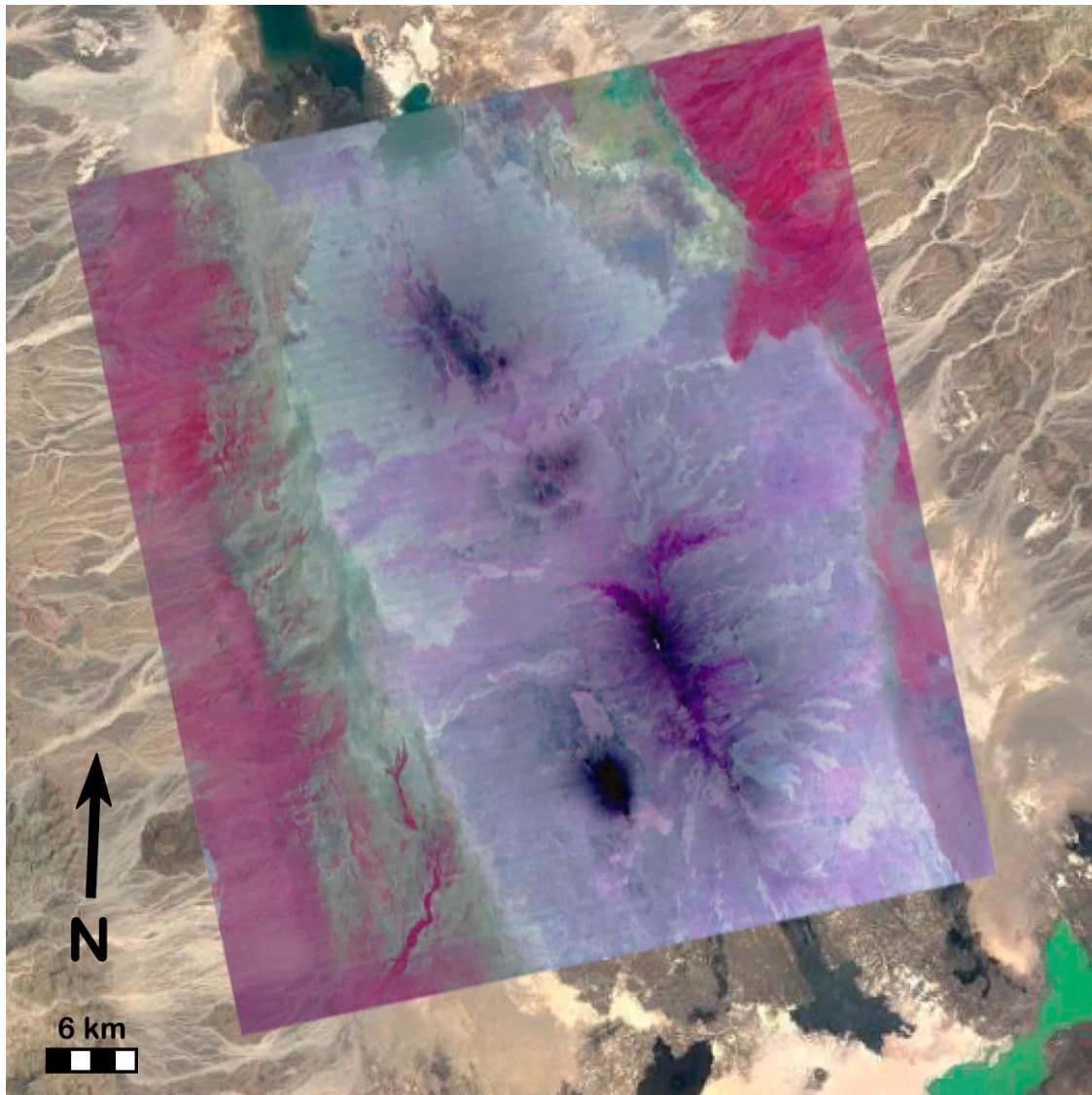


Figure 1. The first Advanced Spaceborne Thermal Emission and Reflection Radiometer (ASTER) multispectral thermal infrared (TIR) image acquired on 6 February 2000, before the start of the instrument's science operational phase. Erta Ale volcano, Ethiopia (summit location: 13.60°N, 40.67°E), is shown using a decorrelation stretch (DCS) of the TIR bands 14, 12, 10 in red, green, and blue, respectively. Color variations are mainly caused by rock and soil compositional differences, and only possible with the ASTER multispectral TIR data. The blues and purple colors are indicative of dominantly basaltic lava flows. The small cluster of white pixels in the lower central part of the image is the summit lava lake thermal anomaly. The ASTER DCS data are overlain on a visible Google Earth image for context. Image credit: NASA/METI/AIST/Japan Space Systems, and U.S./Japan ASTER Science Team.

1.2. Twenty Years of Volcanic Studies Using ASTER Data

The ASTER Science Team created useful derived science products that have benefited numerous scientific fields such as volcanology. These include a robust temperature emissivity separation algorithm for the first orbital high spatial resolution multispectral TIR data [8], programs such as the Science Team Acquisition Request (STAR) to acquire data focused on important science questions of individual users/teams, as well as the ability to generate DEMs [9]. These individual-scene DEMs of 60 by 60 km were later composited globally into the ASTER Global DEM or GDEM—version 3 of which was released in August 2019 [10,11].

Arguably, volcanology is one of the scientific disciplines on which ASTER data have had the greatest impact. In order to quantify this impact and gather all volcanology related studies together into one reference document, we have performed an extensive literature review (Appendix A). This found 271 peer-reviewed publications from 1 January 1995 to 1 December 2019, an average of nearly 11 per year (Figure 2). Papers published prior to the Terra launch were considered precursory studies, commonly describing how the future ASTER data would be used for certain volcanic studies. This list of 271 publications was subdivided into 12 categories based on the volcanic focus of the papers. The category names and number of papers in those categories (shown in parentheses) are: Analogs (3), Calibration (4), Lava Flows (4), Gas/Plumes (30), Geothermal (9), Mapping (54), Modeling (16), Monitoring (96), Operational (4), Other (4), Precursory (16), and Topography (31). Based on this categorization, ASTER data have been primarily used to monitor volcanic activity; somewhat surprising considering the lower temporal frequency of the data. This speaks to the need for future high spatial, high spectral resolution data at temporal resolutions far better than the nominal 16 day equatorial repeat time of ASTER and Landsat, or even the 5 day resolution of the Sentinel-2 constellation. This same finding was also brought forward in the most recent Decadal Survey for Earth Science, which noted data such as these are critical for addressing two of the most important science questions related to natural hazards [12].

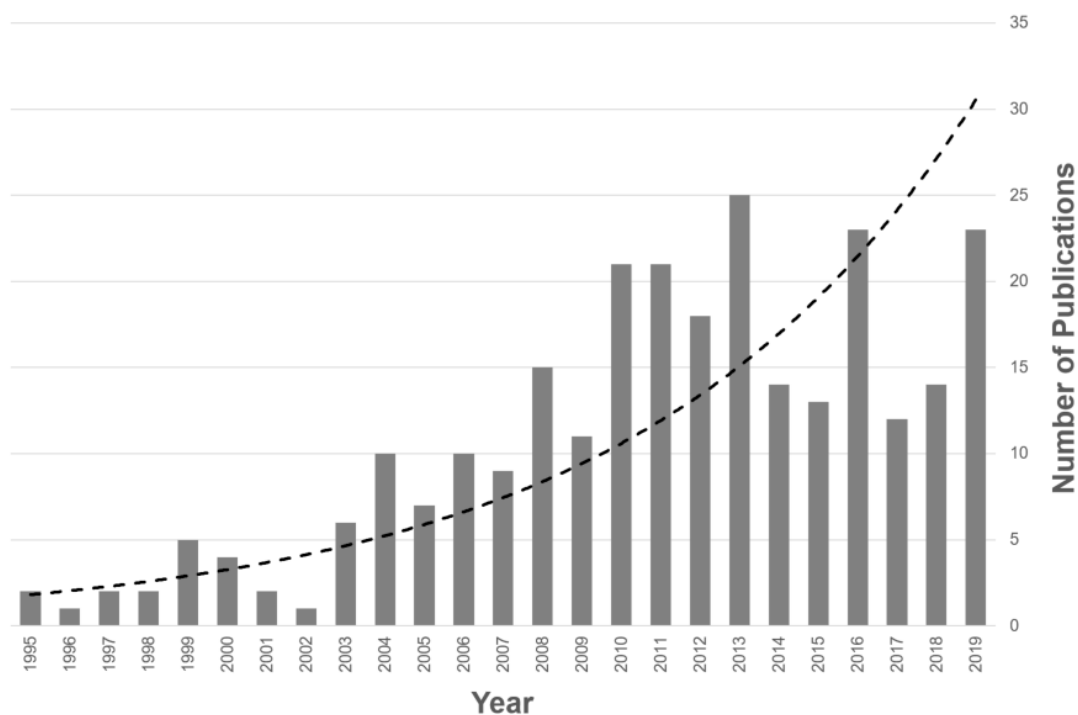


Figure 2. The number of volcano-related publications per year that have incorporated ASTER data in some aspect of the work. Through 2016, the growth has been roughly exponential (dashed line). That growth has declined somewhat in the last several years, although still remaining respectable. The total number of publications shown is 271, spanning the last 25 years.

2. Background

2.1. Volcanological Remote Sensing

The data from spaceborne sensors used to detect, monitor, and even forecast eruptions have been analyzed since the earliest days of the satellite era, e.g., [13–15]. Those early studies using the data available at the time focused mostly on hot spot detection and temperature measurements with TIR data. The studies continued to expand despite the fact that no sensor launched by any country has ever been specifically devoted to volcano science. Scientific studies grew ever more complex with the launch of new sensors providing better spatial, temporal and spectral data, arguably creating the field of spaceborne volcanology. The ability to extract critical information from subtle phases of precursory activity in order to perform the detailed spectral mapping of the erupted products grew exponentially [16]. Many of these studies describe the detection of a new thermal anomaly at a quiescent volcano, which gave rise to models of the sub-pixel temperature distribution. High temporal temperature data allowed more accurate modeling of lava and gas flux rates as well as chronological descriptions of each eruptive phase. Ramsey and Harris [17] summarized the history of satellite-based TIR research of active volcanoes into four broad themes: (1) thermal detection, (2) analysis of sub-pixel components, (3) heat/mass flux studies, and (4) eruption chronologies. Ramsey [2] added a fifth theme, the creation of sensor webs consisting of integrated data from multiple sensors to improve the spatial and/or temporal resolution.

Volcanology, as is the case for many other disciplines relying on orbital image data, adapted to the fundamental technological divide of the availability of high temporal/low spatial resolution versus that of low temporal/high spatial resolution data. Volcanological processes operating at the minute to hourly time scale (e.g., lava effusion, plume emplacement, drifting ash clouds) require data very different than those acquired on the time scale of days to weeks. The former falls under a class of TIR sensors designed primarily for weather and atmospheric studies and includes sensors such as the Advanced Very High Resolution Radiometer (AVHRR), the Along Track Scanning Radiometer (ATSR), the Moderate Resolution Imaging Spectroradiometer (MODIS), the Visible Infrared Imaging Radiometer Suite (VIIRS), as well as instruments on the Geostationary Operational Environmental Satellites (GOES). These sensors are commonly designed with wide swath widths, a limited number of spectral bands, and spatial resolutions of 1.0 km/pixel or larger, which result in temporal frequencies of minutes to hours. Modeling the data to extract information below the scale of the pixel have made these datasets invaluable for both the rapid detection of new activity as well as the analysis of time-scale dependent eruptive processes [18–20].

TIR data of the Earth's surface evolved from very coarse spatial resolution to the sub-100 m scale, and from one spectral channel for temperature measurements to five for the ASTER and ECOSystem Spaceborne Thermal Radiometer Experiment on Space Station (ECOSTRESS) instruments. This class of sensors includes instruments on the current Landsat platforms as well as older systems like ASTER and newer ones such as ECOSTRESS. These commonly have a larger number of spectral bands than the weather class of sensors, spatial resolutions of 100 m/pixel or better, but a temporal frequency of days to weeks. The improved spatial and spectral resolution does provide for studies of smaller-scale volcanic processes with detection of much smaller temperature variations, e.g., [3,5,21]. These sensors are also excellent for detecting early precursory activity despite the infrequent coverage, e.g., [22]. However, the data cannot be used to describe the high-frequency changes ongoing during an eruption despite providing a detailed "snapshot in time" of that activity.

2.2. The 2018 Decadal Survey Recommendations

Land surface image data at ever-improving spatial, spectral and temporal scales, which also span a wide wavelength range from the VNIR to the TIR, have greatly improved our understanding of geological and biological processes operating at those observational scales. This has been recognized for decades with Landsat data, which have been improved spatially and spectrally as changes were

made to the instrument design. Following its launch, ASTER data greatly increased both the spatial and spectral ranges, providing new capabilities from that of Landsat, significant especially for volcanology.

The need to continue (and improve upon) this class of measurement was recognized in the first Decadal Survey (DS) for Earth Science in 2007 [23]. In that report, a notional list of mission concepts was proposed, which included the Hyperspectral Infrared Imager (HyspIRI) mission that paired a hyperspectral visible/shortwave infrared (VSWIR) instrument with a multispectral TIR instrument. Many years of planning, design and science concept studies were later performed. Ultimately, however, the mission was never selected by NASA to move forward and the concept study was formally ended with the publication of the second Decadal Survey in 2018 [12].

The second report focused on science questions and key observables, around which new mission concepts could be structured. Notably, the lack of future global TIR and VSWIR image data was once again brought forward in the new DS report. For example, the requirement for infrared measurements spanned all of the working group panels, being mentioned over 190 times in the report and 12 times in the requests for information from the general science community. Focusing specifically on the reports of the Ecosystems and the Earth Surface and Interior panels, which contributed most directly to the need for TIR data, those data were key inputs for 14 different science objectives—half of which were designated as “most” or “very” important, the top categories. The science and applications summary includes the need for measurements of surface geology, active geologic processes such as natural disasters, surface/water temperature, as well as functional traits of vegetation and ecosystems. The Earth Surface and Interior panel, for example, focused two of its top-level science questions on natural disasters: data prior to the event and the outcomes following. TIR measurements are noted as vital for several of these disasters, including volcanoes, landslides and wildfires. Although temperature is an important measurement, the need for vast improvements in TIR spatial, spectral and temporal resolution data was made clear. TIR data acquired in 1–2 channels at 100 m resolution every 2 weeks no longer satisfies the requirements deemed important by the science community for the future. Hyperspectral TIR coupled with vastly improved temporal resolution at spatial scales exceeding current ASTER capabilities were recommended. The DS report lists several Designated Observables (DOs), including the Surface Biology and Geology (SBG) DO. A mission concept designed to address this DO will likely include some combination of these recommended scales of TIR data, which will allow far more detailed volcanic measurements than currently possible with either ASTER or Landsat data.

3. The Methodology of ASTER Volcano Observations

3.1. The Need for More Routine ASTER Volcano Observations

3.1.1. The ASTER Volcano Science Team Acquisition Request (STAR)

The recognition that ASTER data would provide a fundamentally new tool for volcanic observations was documented even before the Terra launch [7]. During that development period, the ASTER Science Team (AST) foresaw that the instrument would eventually provide data at spatial and spectral scales never before observed, routine data at night, the ability to point off-nadir to improve temporal revisit time, and therefore, required daily observation schedules. Being a scheduled instrument, unlike many other nadir-viewing systems, brought both a higher level of mission complexity as well as unique opportunities for Earth observations. Scheduling allowed specific ground targeting, a focus on larger-scale global processes, as well as an important goal of creating a global map of ASTER data.

One observational and scheduling strategy developed was the creation of the science team acquisition request or STAR. The STARs are a series of globally distributed regions of interest (ROIs) over targets with high scientific value. The ROIs had associated attributes such as seasonality, instrument gain settings, number of observation attempts per year, etc. These targets were integrated into the daily scheduling so that both STAR-focused scenes were acquired together with the many other required observations during any given orbital period. The STAR's assured a priority set of

observations for high-interest science such as monitoring the global land ice inventory, change detection of large urban environments, and volcanic activity [24–26].

The ASTER Volcano STAR's scheduling plan was designed to allow routine observations over the world's volcanoes, which were then made available to the scientific community as quickly as possible [26]. The original plan divided the global list of the approximately 1000 active and/or potentially active volcanoes into high, medium and low priority classes. These divisions, initially dubbed class A, B, and C, respectively, varied according to the historical frequency of their eruption activity. Class A consisted of volcanoes that had several recorded eruptions during the prior decade; class B volcanoes had several recorded eruptions during the past several decades; and class C consisted of the remainder of volcanoes that had not seen activity in the prior century. The STAR designated that class A targets would be observed every 48 days during the day and every 32 days at night. Class B targets were to be observed every 3 months, both in the day and night. Finally, class C targets were to be observed once every 6 months [27,28]. Although this plan continues to provide regular data of all the volcanoes on Earth, many eruptions and the precursory activity prior, were missed due to this schedule rigidity. For the Volcano STAR, ASTER acquires ~16,000 scenes per year on average, which is a combination of day and nighttime data, for a total of ~320,000 individual ASTER volcano scenes over the mission lifetime. Therefore, for the 964 individual volcano ROIs in the ASTER Volcano STAR, each volcano is observed ~16 times per year on average. Although an improvement over the nominal observational schedule, this frequency is still not enough to allow rapid response observations nor discrimination of short-timescale activity, especially considering that some percentage of these scenes are dominated by clouds.

3.1.2. The ASTER Urgent Request Protocol (URP)

Because of the lack of an adequate temporal sampling of the very restless and actively erupting volcanoes with the volcano STAR, the ASTER Urgent Request Protocol (URP) Program was proposed [2,29]. Simply, the URP is a means to improve the number of observations at the most active volcanic centers around the world. The URP integrates ASTER into a sensor web construct where all scales of activity at an erupting volcano can be captured [29,30]. The initial and most straight-forward implementation of this approach for the URP uses detection of thermally elevated pixels in high temporal resolution data to subsequently trigger more rapid scheduling and acquisition of the higher spatial/spectral resolution data from ASTER. With such a system in place, the high-frequency activity can be continually imaged throughout the eruption, with the high spatial resolution data ideal for capturing small scale changes. These ASTER data also serve as validation for the low spatial, high temporal resolution data.

The URP program has been in place as part of the ASTER sensor's operational scheduling since 2005 [2,29], responsible for over 5000 additional scenes of active volcanoes during that time (one new scene on average every day). Perhaps more importantly, the URP can be triggered manually if precursory activity is noted based on ground-based observations or reports. This allows pre-eruption data to be acquired that significantly add to the monitoring process [22].

Later expansion of the URP Program increased the original monitored area from the northern Pacific region to the entire globe [2]. The URP currently operates with two global monitoring systems using MODIS data: MODVOLC [31] and Middle InfraRed Observation of Volcanic Activity (MIROVA) [32] as well as AVHRR data focused in the north Pacific region using the Okmok algorithm [33]. New triggering systems are now being tested that will integrate ground-based thermal camera data as the source for new URP data. A trial system at Mt. Etna volcano in Italy has been ongoing since mid-2019 and will expand to Piton de la Fournaise volcano on Réunion Island in 2020 using seismic alerts as the triggering source. The addition of the URP to the ASTER observation schedule is a vast improvement from the original volcano STAR [3,27]. Importantly, however, the URP operates in tandem with the volcano STAR. The volcano STAR data represent additional scenes for the very active volcanoes, thus supplementing the URP archive. Conversely, the volcano STAR data are commonly the only information for the less active, non-thermally elevated targets, and therefore continue to represent an important source for global volcano data.

3.2. Volcano Data Archives

3.2.1. The ASTER Image Database for Volcanoes

The entire ASTER archive is available at the Land Processes Distributed Active Archive Center (LP DAAC), which can be searched using tools such as EarthDATA and GloVis (Table 1). Other web-based data repositories, however, have been created specifically for the volcano data products. The first of these is the Image Database for Volcanoes (IDV), which was created by M. Urai, and is located in and served from Japan [27,34]. A new volcano image is commonly added within a week of acquisition. The database contains all ASTER images of the 964 target volcanoes that comprise the ASTER Volcano STAR. A 20 km² area centered on the geographic location of volcano is shown and stored in the database. Links to each volcano are also displayed and upon selection, the best VNIR image, geographic information, and a table ordered by date of all the acquisitions are shown. The chronological list has thumbnails of the each of the three ASTER imaging systems (where available) along with metadata links for access and download.

Table 1. Volcano-specific data archives and search tools available for all ASTER data.

Site Name	Site Web Address and Relevant Information
Land Processes Distributed Active Archive Center (LP DAAC)	https://lpdaac.usgs.gov/data/get-started-data/collection-overview/missions/aster-overview/ Contains the entire ASTER archive from 2000 to present, including the on-demand higher-level data products
Image Database for Volcanoes (IDV)	https://gbank.gsj.jp/vsldb/image/index-E.html Contains a 20 km ² area around each of the 964 volcanoes in the ASTER Volcano STAR database, for the entire mission from 2000 to present
ASTER Volcano Archive (AVA)	http://ava.jpl.nasa.gov Contains the full ASTER scene in multiple formats for ~1500 volcanoes, in addition to other sensor data and derived products. Archive currently spans from 2000 to 2017
EarthDATA Search Tool	https://earthdata.nasa.gov/ Searchable visual archive for the entire ASTER mission from 2000 to present, including the on-demand higher-level data products
GloVis Search Tool	https://glovis.usgs.gov/ Searchable visual archive for the entire ASTER mission from 2000 to present

Urai [34] conducted an initial evaluation of the ASTER Volcano STAR performance using data in the IDV. As expected, volcanoes in Iceland and Kamchatka were observed the most frequently. At the time of the study, 77% of all the volcanoes in the database had at least one daytime image with <10% cloud cover. The IDV remains active as of the time of this writing, and as of the latest IDV update on 1 December 2019, the average number of scenes acquired had grown to 146.3 (daytime) and 185.4 (nighttime) per volcano.

3.2.2. The ASTER Volcano Archive (AVA)

The second online volcano database to appear was the AVA, which is housed and served in the United States at the Jet Propulsion Laboratory [27,28]. The AVA is the largest dedicated archive of web-accessible volcano images now containing image data other than ASTER as well as secondary derived products for each volcano (Table 1). The archive provides capabilities to inventory and monitor properties and processes over time. These include the spectral signatures for volcanic emissions (e.g., eruption columns and plumes) and surficial deposits (e.g., lava flows, pyroclastic flows), as well as eruption precursor data. AVA has helped to improve the global monitoring and access to archival ASTER image data of more targets (~1500) than are in the ASTER Volcano STAR. Much like the IDV,

volcanoes can be searched by name or location, and thumbnail images. Unlike the IDV, AVA data can be downloaded as full ASTER scenes in geoTIFF, KML, or HDF formats. These data can be also combined with the DEM files and ancillary data in an easily accessible format, which is useful in organizing the multispectral geological analysis of a particular volcano [35]. As of this writing, however, no new data have been added to the archive since late 2017. This is scheduled to be reactivated sometime in 2020.

3.3. Operational Structure of the Ongoing ASTER Volcano Observations

All ASTER data acquired as part of ongoing routine Earth observations (i.e., the Volcano STAR, global map imaging, etc.) are archived at the LP DAAC. These data are stored in several formats including raw radiance at sensor, from which numerous level 2 data products (e.g., digital elevation model, surface TIR temperature), can be ordered as on-demand products. Image data that fulfill the requirements of the Volcano STAR are also assessed weekly and stored in the IDV and the AVA archives, the latter until 2017. These volcano archives allow quick data searches on particular volcanoes and visualizations of the latest data, whereas the LP DAAC archive contains all the data, all possible level 2 options and the most up to date processing levels for each on-demand product.

Data collected as part of the URP Program are also eventually stored in the LP DAAC ASTER archive and are pulled over to the individual volcano archives as well. However, because of their expedited classification, these data are processed quickly into the Level 1BE (expedited) format and staged on the expedited data system webpage at the LP DAAC for immediate download and assessment. Within 2 h of the data being acquired, all scientists involved with the URP Program are automatically notified by email and have immediate web-based access to the new scene. Any significant changes detected in the data of a particular eruption are disseminated to the responsible monitoring agencies, local scientists working on the eruption, as well as the global community through e-mail and mailing lists. More detailed science analysis is then commonly performed over time and with the arrival of new data. All new, newly scheduled, and ongoing volcano observations of each URP volcano are tracked both through a database and email system as well as web-based map tool showing all the current targets color coded by ASTER observations status (Figure 3). Each color coded pin is clickable allowing a query of the latest observations and links to the metadata for each scene. Also shown is the current position of the Terra satellite.



Figure 3. The ASTER Urgent Request Protocol (URP) Program scheduling interface using Google Maps, and maintained at the LP DAAC. All currently monitored URP target volcanoes are shown with a color-coded pin. These are updated automatically when new targets are triggered or existing ones have a change of status. Each pin is clickable to display more information and links to other metadata. The position of the Terra spacecraft and its orbit tracks are also shown.

3.4. Statistical Analysis

All ASTER scenes used in this study were acquired from the LP DAAC through the NASA EarthData web-based search tool using an initial search refinement by date. The refined datasets were then downloaded as ASTER Level 2 surface kinetic temperature (AST_08) products. This data product allows the most efficient way to identify volcanic activity by temperature within a given scene. Scenes were automatically scanned and later visually inspected for any thermal variations. If no activity was initially identified, a more detailed investigation for thermally elevated pixels was performed for each scene. If this process yielded a negative result, the scene was classified as having no detectable volcanic activity. If volcanic (thermal) activity was present, then the type of activity was classed as a plume, lava flow, other flow, or summit hot spot. The cloud cover percentage was also visually determined for all the scenes investigated. This was then compared to the ASTER Cloud Cover Assessment Algorithm (ACCAA) value for future assessment analysis.

4. Results

4.1. ASTER Capabilities and Observation Strategies

The unique instrument characteristics that make ASTER particularly well suited for volcanic observations include multispectral TIR data, routine TIR data at night, high spatial resolution data, variable gain settings to limit data saturation, off-axis pointing, and generation of along-track digital elevation models [3,36]. For example, the multispectral TIR data at a relatively high spatial resolution allowed a variety of surface materials to be distinguished and a better understanding of thermal and compositional mixing at the sub-100 m pixel scale [6,37,38]. The following are examples particularly relevant to each of the ASTER instrument characteristics. For a complete list of all ASTER-specific volcanological papers, see Appendix A.

4.1.1. Routine TIR Data at Night: Elevated Temperatures at Fuego Volcano, Guatemala

Unlike other orbiting instruments of similar spatial and temporal resolutions, ASTER routinely acquires TIR data at night. In certain special observational modes (e.g., large and highly radiant lava flows), VNIR nighttime data can also be acquired. Nighttime TIR have the advantage of reduced residual solar heating, reduced thermal topographic effects, and typically have lower cloud percentages compared to daytime scenes [3]. Subtle thermal anomalies are therefore more easily identified in nighttime TIR data. A new study by Flynn and Ramsey [39] of Fuego volcano from (1 January 2000 until 30 April 2018) found that ASTER acquired 308 scenes—193 of which were collected at night. Of those nighttime scenes, 109 had visible volcanic activity present, with 47 being summit hot spots and 62 showing either lava flows or pyroclastic density currents (PDCs). These data were compared to the Guatemalan monitoring agency's weekly reports to determine the specific volcanic event that could have caused the thermal detections in the ASTER data. This data synthesis is then used to create volcanic hazard maps and cross check datasets for missed events. Without the nighttime TIR data, many of these volcanic events may not have been observed.

4.1.2. Multispectral TIR Data: SO₂ Plumes from Lascar Volcano, Chile

The multispectral resolution of the ASTER TIR data enabled Henney et al., [40] to detect and measure very low SO₂ concentrations (<1 g/m²) released from Lascar volcano in December 2004 (Figure 4). Of note by the authors was the high spatial resolution and radiometric sensitivity, which along with the needed multispectral resolution allowed these retrievals of very small SO₂ burdens, which are not possible with any other orbital instrument. The TIR results were also compared to ground-based measurements made in the ultraviolet (UV) spectral region during a coordinated overpass of ASTER and found to be well within the error of those instruments.

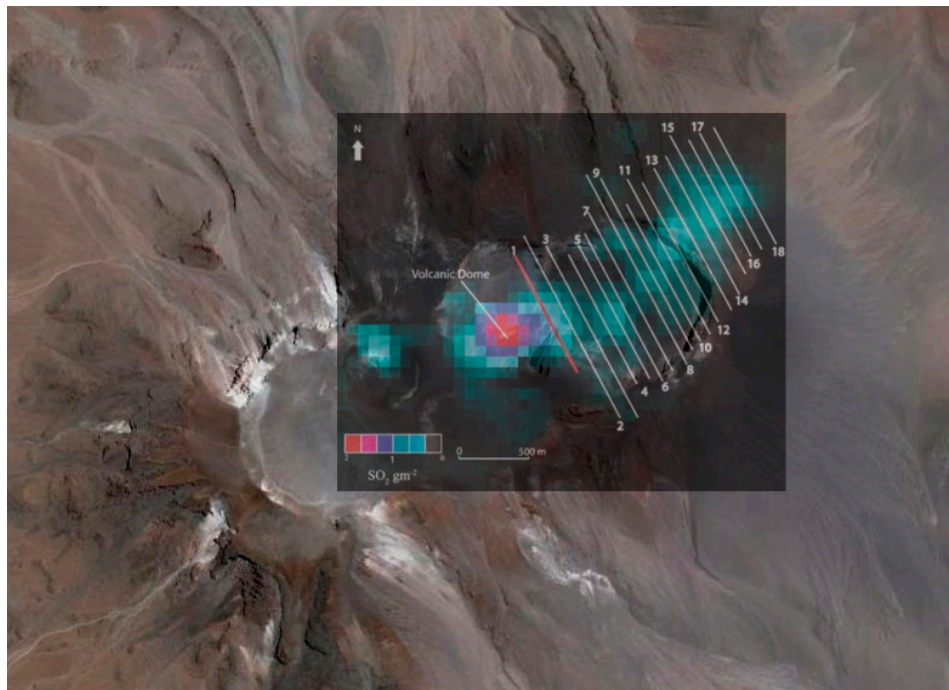


Figure 4. The map of the very low SO_2 burden retrieved using ASTER TIR data acquired at Lascar volcano, Chile (summit location: 23.37°S , 67.73°W) on 7 December 2004. Image is draped on a visible Google Earth image for context. Numbered lines indicate transects taken through the plume and reported in the original study. SO_2 results were created using the Map_ SO_2 software of Realmuto [41] and each color bin corresponds to $\sim 0.3 \text{ g/m}^2$ of SO_2 . Figure modified from Henney et al. [40].

4.1.3. High Spatial Resolution Data: TIR Analysis of Hawaiian Volcanoes

The high spatial resolution of the ASTER data, in particular in the TIR, was documented by Patrick and Witzke [42] for long-term mapping and monitoring of the active or potentially active volcanoes on the islands of Hawai'i and Maui. The goal of the study was to determine the baseline thermal behavior over ten years (2000–2010) in order to assess thermal changes that may precede a future eruption. They used cloud-free kinetic temperature ASTER data acquired for the five major subaerial volcanoes in Hawai'i (Kilauea, Mauna Loa, Hualālai, Mauna Kea, and Haleakalā). The data were geolocated and stacked to create time-averaged thermal maps and to extract temperature trends over the study period. Conspicuous thermal areas were found on the summits and rift zones of Kilauea, Mauna Loa, and the small pit craters on Hualālai. No thermal areas were detected on Haleakalā or Mauna Kea. One limiting factor noted for the lack of detections was the pixel size of the ASTER TIR, which despite being one of the highest from orbit, was seen as still too large to detect possible subtle thermal changes as well as to identify small-scale, low-temperature thermal activity.

4.1.4. Variable Gain Settings (VNIR/SWIR): High Temperature Monitoring of Klyuchevskoy Volcano, Russia

The ASTER VNIR and SWIR (no longer functioning) subsystems both have/had the ability to acquire data at different data gain settings. The VNIR has three settings (low, normal, and high), whereas the SWIR had four (low1, low2, normal, and high). These gain settings must be set prior to scheduling an observation, so some degree of advanced knowledge of the target is required. They were created to limit data saturation in regions of excessively high or low radiance (e.g., bright glacier and clouds surfaces, dark water body surfaces, etc.). Typically, these gain settings are uniformly set across all bands in the VNIR and the SWIR (when it was operating). However, a unique scenario was created for the volcano STAR whereby every other SWIR band was alternated between the normal and the low2 gain settings in order to maximize the possibility of capturing some unsaturated data

of a future volcanic target that may have lava on the surface [25]. The saturation pixel-integrated brightness temperature for the SWIR ranged from 86 °C in band 9 (*wavelength* = 2.336 μm and *gain* = *high*) to 467 °C in band 4 (*wavelength* = 0.804 μm and *gain* = *low2*). For the VNIR, the range is 669 °C in band 3 (*wavelength* = 0.807 μm and *gain* = *high*) to 1393 °C in band 1 (*wavelength* = 0.556 μm and *gain* = *low*). By comparison, the TIR has only one gain setting and a saturation pixel-integrated brightness temperature of 97 °C.

These variable gain settings have proven quite useful for deriving accurate pixel-integrated brightness temperatures of large, highly radiant lava flows over the ASTER mission lifetime. For example, Rose and Ramsey [43] describe the use of all three ASTER subsystems to monitor the emplacement of multiple long lava flows at Klyuchevskoy volcano, Kamchatka during the 2005 and 2007 eruptions. In 2007, temperatures were extracted from 4 January to 7 June 2007 and fit into the volcanic warning color codes over that period (Figure 5). For the first 4.5 months of the eruption, TIR data remained unsaturated and the SWIR-derived temperatures, acquired in high-gain mode, were only detectable in the highest SWIR wavelengths. This corresponded to the time period that Klyuchevskoy was designated with yellow and orange color codes, signifying increasing levels of restlessness, but no eruption. From 26 April to 10 May, all TIR and SWIR-derived temperatures became saturated due to the emplacement of new open-channel lava flow that was radiant enough to be detected at the 15 m VNIR spatial scale. VNIR-derived temperatures (852–895 °C) were detected for the first time in the eruption. These detections took place one week before the alert level was raised to red (signifying an active eruption), attesting to the importance of high-repeat, non-saturated data for the monitoring of these more remote volcanoes.

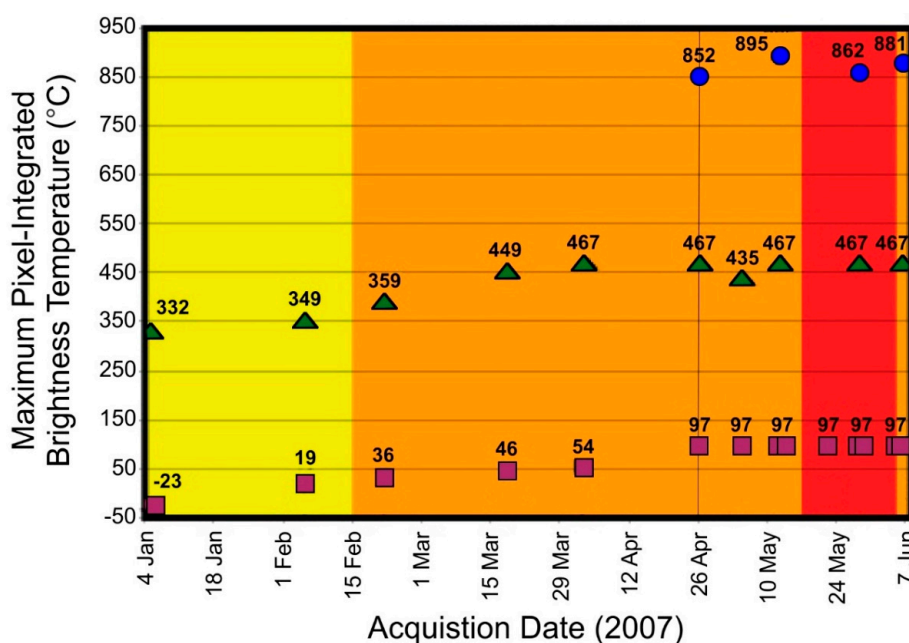


Figure 5. Maximum ASTER-derived pixel-integrated brightness temperatures detected during the 2007 eruption of Klyuchevskoy volcano, Russia. Thermal infrared (TIR) temperatures are denoted with purple squares; shortwave infrared (SWIR) temperatures with green triangles; and visible/near-infrared (VNIR) temperatures with blue circles. The background colors represent the volcanic color code issued by the monitoring agencies (yellow = elevated unrest above known background levels; orange = heightened unrest with increased likelihood of eruption; red = eruption is forecast to be imminent). TIR and SWIR temperatures become saturated (and VNIR temperatures become measureable) near the time shown by the thin vertical line. This saturation indicates that a significant amount of highly radiant lava is on the surface and occurred despite adjustments to the SWIR gain settings. Importantly, this was more than two weeks before the color code is changed to red. Modified from Rose and Ramsey [43].

4.1.5. Off-Axis Pointing Capability: Improved Observational Frequency at Piton de la Fournaise Volcano, France

During the April–May 2018 eruption of Piton de la Fournaise volcano on Réunion Island, satellite-based surveillance of the thermal activity and emitted plumes was paired with near-real-time flow modeling to create an ensemble-based approach in response to the crisis [44]. This combined effort of four institutions in several countries using data from numerous sensors to model and forecast lava flow advance was done as a proof of concept in order to assist the small staff of the volcano observatory on the island. Rapid data acquisition was critical and provided by MODIS via the MIROVA system to determine lava discharge rates. The less frequent but higher spatial resolution ASTER data were important both for determining the length, shape and direction of the flow using the TIR data (Figure 6), as well as the precise location of the vent using the VNIR data. The TIR images served as a validation for the MODIS data and the predicted down slope flow modeling, whereas the VNIR-derived vent location was used as the initiation point for the flow modeling, critical for model accuracy. During the 35 day eruption, a total of 11 ASTER images were acquired. This average of ~1 image every 3 days was a significant improvement over the nominal 16 day repeat time for targets close to the equator. The improved temporal resolution was only made possible with the ASTER URP Program and the off-nadir pointing capability of 8° nominally and up to 24° for the VNIR.

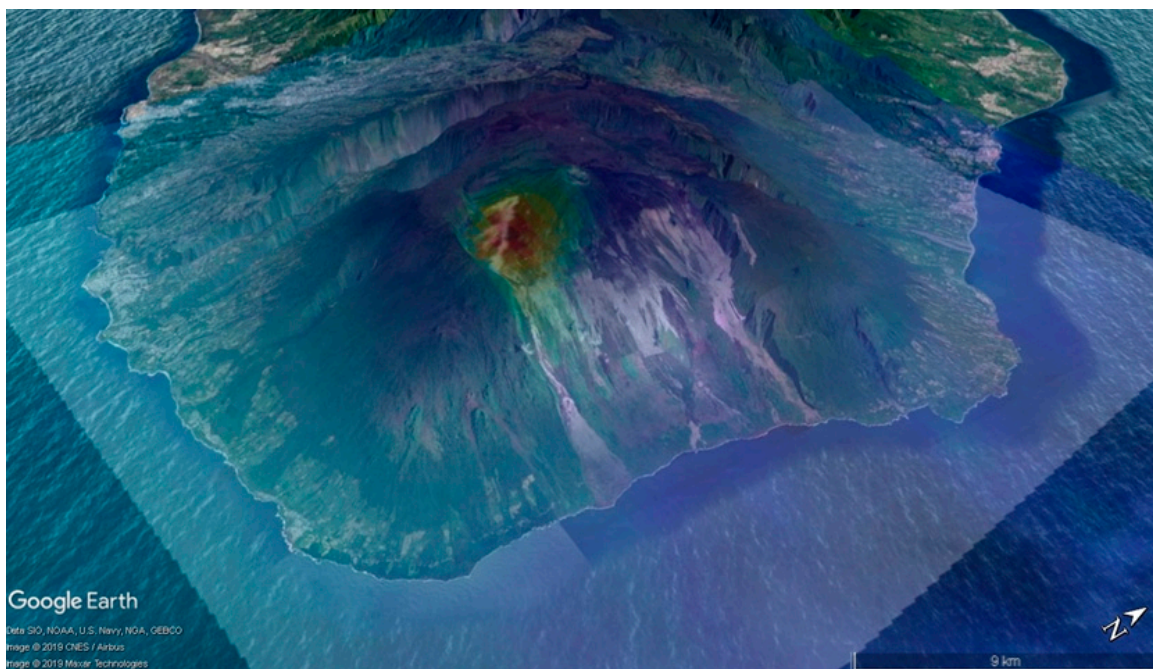


Figure 6. Piton de la Fournaise volcano, Réunion Island (summit location: 21.24°S, 55.71°E) during the April–May 2018 eruption crisis. Image/data modified from Harris et al. [44]. A color-coded Moderate Resolution Imaging Spectroradiometer (MODIS) radiance image produced by the Middle InfraRed Observation of Volcanic Activity (MIROVA) monitoring system is draped over a 3D Google Earth visible image for context. These KML image products are routinely produced by MIROVA. Draped on both data sets is the nighttime ASTER TIR data acquired as part of the URP Program. The ASTER image, acquired 6 days after the triggering MODIS detection, shows the spatial details of the propagating lava flow as the brighter white pixels within the colorized MODIS pixels.

4.1.6. Generation of Along-Track Digital Elevation Models (DEMs): Volcanoes in Guatemala, New Zealand, and Mexico

The ability to produce single 60 by 60 km scene DEMs from any daytime VNIR data is another significant capability of the instrument. Importantly, these data provided digital topography for most of the Earth's land surface at 10 m accuracy early in the mission when such information was not

available from other data sources such as radar. Later in the mission, these individual-scene DEMs were compiled into a seamless global data set known as the ASTER Global DEM or GDEM. The GDEM has better signal to noise and removes areas of clouds or other artificial errors commonly found in the single-scene DEMs (Figure 7). The final version (v.3) was released in August 2019 having corrections made to minor areas of known errors.

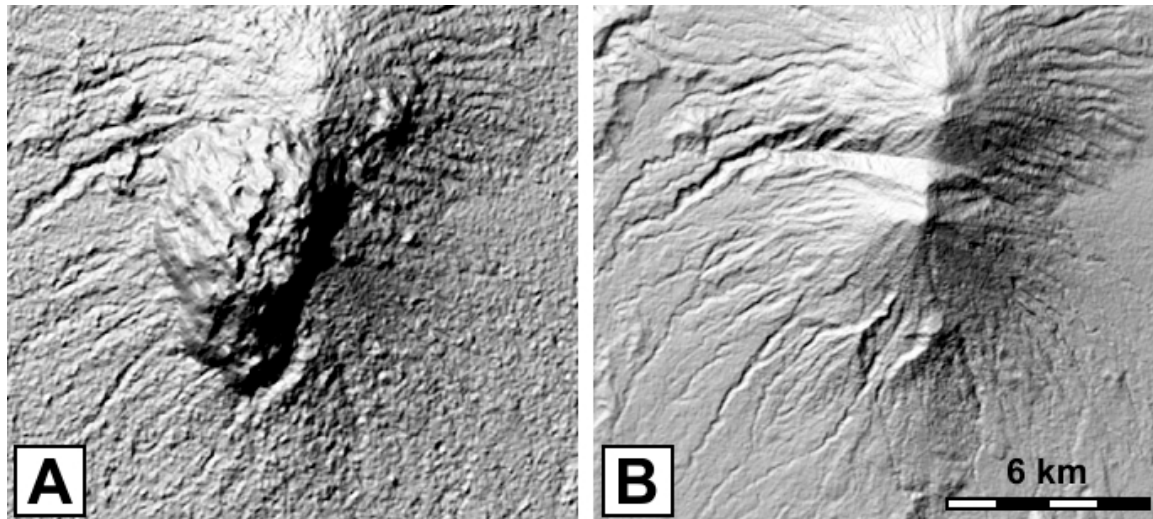


Figure 7. Examples of ASTER-derived DEMs for Fuego Volcano, Guatemala (summit location: 14.48°N, 90.88°W). (A) Single-scene DEM from VNIR data acquired on 10 December 2018. Clouds are causing the erroneous topographic high that obscures the summit and central crater. The pixel to pixel noise is also clearly visible. (B) ASTER GDEM v3 using only cloud-free scenes and greatly improving the signal to noise of the DEM.

Whereas the GDEM provides an excellent baseline for volcanological studies reliant upon topography, it does not account for changes to the surface, either during the period used for the GDEM creation (2000–2011) as they would have been averaged out or not included in subsequent data. Dynamic topography is a characteristic of most active volcanoes and accurate knowledge of that topography becomes important for any type of lava or pyroclastic flow forecast modeling. Therefore, current single-scene DEMs continue to be an important dataset for volcanological studies using ASTER. Stevens et al., [45] noted this point in their study examining the accuracy of the ASTER single-scene DEM for Ruapehu and Taranaki volcanoes in New Zealand. They found an average root-mean-squared (RMS) error of ~10 m for the ASTER single-scene DEM compared to digitized 1:50,000 scale topographic maps, and later noted that these data will continue to be relevant for future surface change even as global DEM products from radar systems came online. A later study by Huggel et al., [46] evaluated the ASTER DEM against such a global dataset, the Shuttle Radar Topography Mission (SRTM) DEM. The data were used for lahar modeling on Popocatepetl Volcano, Mexico. They found that although the higher number of errors in the ASTER DEM affected certain models more, both the ASTER and SRTM DEMs were feasible for lahar modeling, but that verification and sensitivity analysis of the chosen DEM is fundamental to deriving accurate hazard maps from the modeled inundation areas.

4.2. URP-Specific Results

ASTER data for a subset of volcanoes over several different time intervals were examined for this study and the significant statistics were compiled. The volcanoes were all continuously (or nearly so) active throughout these periods. The goal of this statistical analysis was to determine the improvement of the URP over the nominal Volcano STAR observations. Further details such as the number of cloudy scenes, the number of scenes with confirmed activity and the days between successive observations were also calculated. The interval periods were: one year (1 June 2018 to 31 May 2019) for 10 volcanoes;

the approximate five-year period of the global URP observations (1 January 2014–31 May 2019) for four of those volcanoes; and the nearly entire period of the ASTER mission (13 April 2000–31 May 2019) for one of those volcanoes.

The average percentage of scenes for all the periods that contained detectable volcanic activity was 47.6%, with a range of 19%–69%. For this same period and number of scenes, the average cloud percentage was 50.5%, with a range from 16% to 84%. Finally, during the last five years of the implementation of the global URP Program, the average days between observations at the four volcanoes studied was 6.5 days, compared to 20.2 days with the Volcano STAR Program, a nearly 200% improvement.

4.2.1. One-Year Analysis

Ten volcanoes were chosen for a statistical analysis over a recent one-year period (Table 2). The volcanoes chosen represent a range of eruptive styles, compositions, and latitudinal distributions (Figure 8). All volcanoes were active during the study period and that activity triggered the ASTER URP observations. The number of triggers (derived from MODIS data by the MODVOLC and MIROVA systems) varied from 36 for Popocatépetl to 837 for the Nyamuragira-Nyiragongo volcanoes. The number of triggers is determined by several factors—the most important of which is the style of activity (i.e., persistently active lava lake versus an intermittently active lava dome) and size of the thermal feature on the ground. These combine to determine the overall emitted radiant power. Other factors contributing to the number of ASTER URP triggers also include the latitude of the target together with the average daily cloud cover. Higher latitude volcanoes will have more overpasses due to the converging orbit tracks of the MODIS sensors and hence, more triggers. Persistently cloudy targets will commonly mask thermal activity, lowering the number of triggers. Average cloud percentage was determined by visual inspection of each URP scene done at the same time as the inspection for volcanic activity.

Table 2. Statistical analysis of ten URP-monitored volcanoes active during one year (1 June 2018 to 31 May 2019). Each ASTER scene was inspected for confirmed/detected volcanic activity (e.g., thermally elevated pixels, presence of a plume) and average cloud cover. The percentage of those URP scenes with confirmed activity is also given and generally correlates to the average cloud percentage.

	Number of URP Triggers	Number of URP Scenes	Detected Volcanic Activity and (%)	Avg. Cloud
Ambrym	138	21	4 (19.0%)	62.7%
Erebus	824	36	16 (44.4%)	84.2%
Erta Ale	760	29	13 (44.8%)	16.0%
Fuego	532	30	16 (53.3%)	32.9%
Nyamuragira-Nyiragongo	837	42	23 (54.8%)	61.9%
Piton de la Fournaise	456	22	5 (22.7%)	44.5%
Popocatépetl	36	22	9 (40.9%)	31.5%
Sangeang Api	251	27	11 (40.7%)	46.8%
Shiveluch	623	29	20 (69.0%)	55.0%
Yasur	209	18	1 (5.6%)	77.6%

These MODVOLC and MIROVA triggers resulted in 276 new ASTER scenes during the one-year period with confirmed volcanic activity in ~45% of those scenes, with the remainder being obscured by clouds. The frequency of ASTER URP scenes increases at the higher latitude volcanoes on the list (e.g., Erebus and Shiveluch) as expected. However, Erta Ale at a much lower latitude had a similar number of observations to those two targets, a function of nearly continuous thermally elevated activity present there during the one-year period.

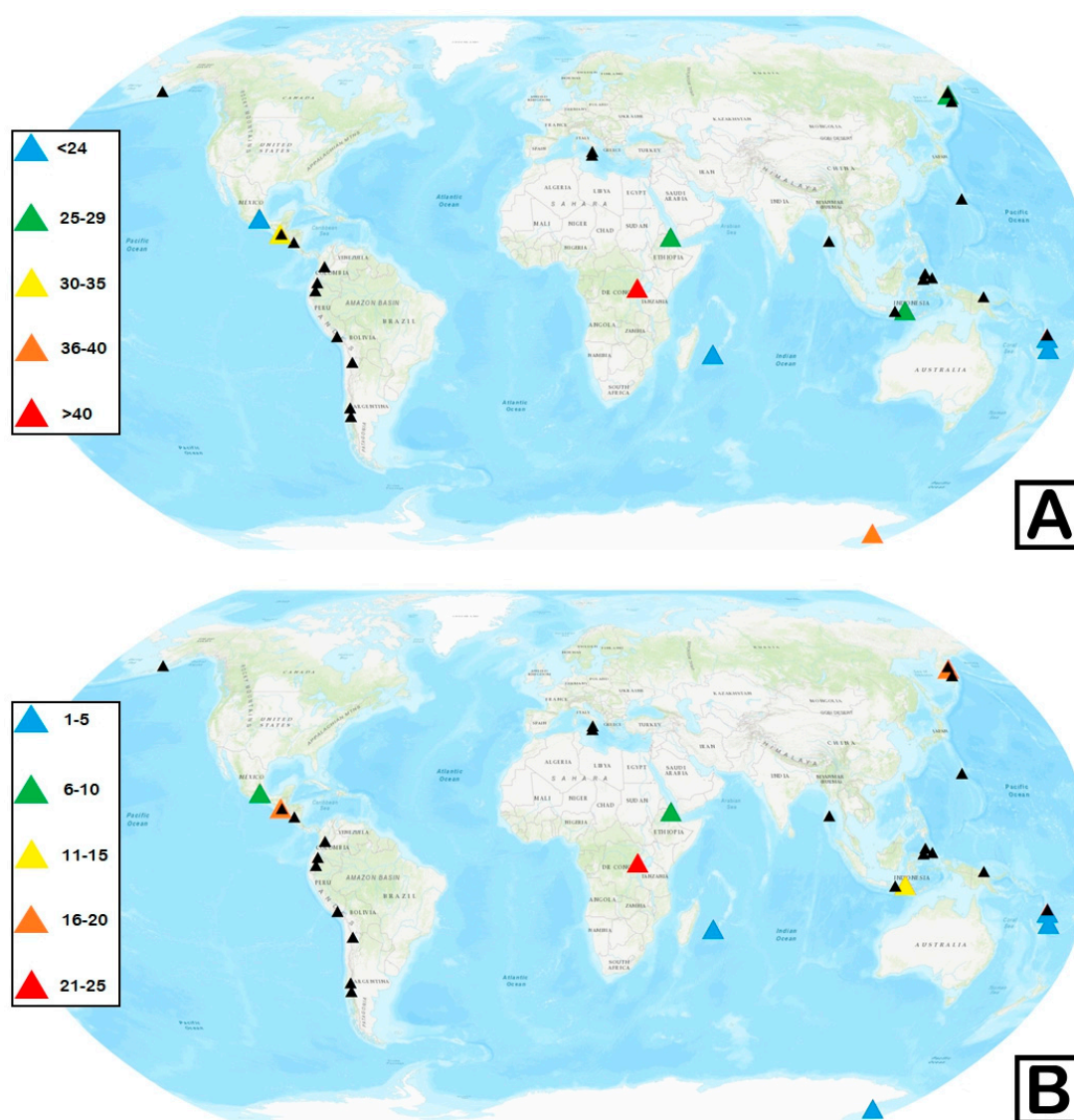


Figure 8. Map of the statistics for the 10 volcanoes detailed in Table 2, which were compiled over 1 year (1 June 2018 to 31 May 2019). Small black triangles indicate active URP-monitored volcanoes at the time, but not analyzed for this study. (A) Number of ASTER scenes acquired. (B) Number of those ASTER scenes with visible volcanic activity.

4.2.2. Five-Year Analysis

Four of the volcanoes in the prior list were then selected for a longer study period of slightly over five years (1 January 2014–31 May 2019). This period begins when the ASTER URP Program became fully global with the integration of the MODVOLC triggering system. The time frame, therefore, provides the most complete global higher temporal resolution ASTER data for any thermally elevated volcano. As such, the statistics for these observations are the most comprehensive analysis available for the planning of future orbital TIR systems, for example (e.g., expected long-term cloud cover, optimal temporal frequency, etc.).

The data for the four volcanoes chosen (Ambrym, Erta Ale, Popocatepetl, Shiveluch) are shown in Table 3. With the exception of Shiveluch, the others are more equatorial. The four do, however, represent a range of compositions (e.g., dacite, andesite, and basalt) and styles (e.g., dome-forming, lava lakes, and flows). A total of 1001 ASTER scenes were downloaded and analyzed for these four targets. Volcanic activity was confirmed in 535 of these (53.5%) with the remainder being too cloud-covered or having no obvious activity visible in the image. Erta Ale had the highest percent of observed activity

(80.2%) whereas Ambrym had the lowest (29.7%), a clear function of the semi-arid, nearly cloud-free location of Erta Ale compared to the tropical, nearly cloud-covered location of Ambrym. Also analyzed was the average days between an observation for the routine Volcano STAR (20.2 days/scene) as compared to those data from the URP Program (6.5 days/scene). This was an average improvement of 215%, with the best improvement (261%) for Ambrym volcano. The URP Program excels at acquiring more data of targets that are commonly cloudy or close to the equator, and therefore typically missed by the routine STAR observations.

Table 3. Statistical analysis of four volcanoes from Table 2 active during the longer global URP period (1 January 2014–31 May 2019). Each ASTER scene was inspected for confirmed/detected volcanic activity (e.g., thermally elevated pixels, presence of a plume) and average cloud cover. The percentage of those URP scenes with confirmed activity is also given and generally correlates to the average cloud percentage. The time between scenes decreases dramatically for the URP operations as compared to the ASTER Volcano STAR. The last column shows this improvement percentage in the number of days between scenes using the URP versus the STAR scheduling.

	ASTER Scenes	Detected Activity/%	Avg. Cloud	Days/Scene (URP)	Days/Scene (STAR)	% Change (URP/STAR)
Ambrym	239	71 (29.7%)	62.0%	6.4	23.0	261.0%
Erta Ale	243	195 (80.2%)	38.6%	4.4	13.2	198.6%
Popocatepetl	313	153 (48.9%)	19.0%	7.0	24.4	247.1%
Shiveluch	206	117 (56.8%)	62.4%	8.0	20.3	153.8%

4.2.3. Twenty-Year Analysis

Finally, one volcano (Shiveluch) was selected for analysis for nearly the entire period (13 April 2000–31 May 2019) that Terra has been in orbit (Table 4). The first ASTER image acquired of Shiveluch was on 13 April 2000, only 40 days after the start of the operational phase. These early scenes of the volcanoes of Kamchatka also captured the products of a large eruption at Bezymianny volcano described by Ramsey and Dehn [47]. Shiveluch has been persistently active nearly the past twenty years (e.g., [6]) and therefore provides a good target for long-term analysis. It was also imaged more frequently early in the mission because of its location at higher latitudes as well as being one of the northern Pacific volcanoes originally monitored in the first phase of the URP Program, which began in 2005 and relying upon AVHRR data for detection triggering [29].

Table 4. Statistical analysis of a single volcano (Shiveluch) from Table 2 active during most of the entire ASTER orbital period (13 April 2000–31 May 2019). Each ASTER scene was inspected for confirmed/detected volcanic activity (e.g., thermally elevated pixels, presence of a plume, etc.) and average cloud cover. The percentage of those URP scenes with confirmed activity is also given and generally correlates to the average cloud percentage.

	ASTER Scenes	Detected Activity/%	Activity (plumes)	Activity (flows)	Activity (hot spot)	Avg. Cloud	Days/Scene (URP)
Shiveluch	815	430 (52.8%)	53	109	268	62.8%	5.1

The analysis results are shown in Table 4. A total of 815 confirmed scenes were downloaded and interrogated. Similar to the prior results, volcanic activity was confirmed in 430 (52.8%) of the scenes. We further analyzed the type of activity seen in those clear scenes. Plumes were noted in 53 (12.3%) scenes, flows in 109 (25.3%), and summit hot spots in 268 (62.3%) scenes. We also examined the impact of the URP Program to acquire more rapid data of eruption activity. The average time between ASTER Volcano STAR observations at Shiveluch is 8.8 days, much lower than the more equatorial volcanoes (~20 days). Implementation of the URP Program, however, reduced this temporal resolution slightly to 6.1 days. If one were to only consider the data following a new URP triggering event,

this value decreases further to 5.1 days. If volcanic activity wanes and then renews, the first ASTER image acquired after a new triggering event may come many days to weeks after the prior image was acquired. Therefore, this lower interval is likely a better metric of the URP operational behavior. It is also close to the theoretical minimum frequency of ASTER for high latitude targets.

5. Discussion

5.1. ASTER as a Volcanological Instrument

ASTER, unlike almost any instrument designed or chosen by a space agency in the past several decades, was first and foremost a geological sensor. The wavelength regions chosen, the placement of the multispectral bands, the multispatial resolution, and the DEM capability are all critically important for geologic surface mapping. Although it was not designed specifically for volcanology, the geologic heritage of ASTER makes the instrument's data well suited for active volcanic monitoring and data collection. Perhaps the only capability missing was a mid-infrared channel for high-temperature detections. This was offset for the first 8 years of the mission with the 2 μm region SWIR data. As originally noted by Pieri and Abrams [3] and later described by Ramsey [2] and herein, six important instrument/data characteristics made ASTER particularly well suited for spaceborne volcanology. These are the multispectral TIR data, routine TIR data at night, high spatial resolution data, variable gain settings in the VNIR and SWIR, off-axis pointing, and generation of DEMs. Individually, these characteristics all have been used for specific volcanic studies. Where combined, these capabilities become much more powerful for addressing pressing questions in volcanology [45,48].

5.2. Toward an Improving Temporal Resolution

ASTER is able to provide data with improved radiometric resolutions (absolute reflectance $\leq 1.3\%$ and absolute temperature ≤ 0.3 K) [7]. Moreover, it provides data at improved spatial (15–90 m) and spectral resolutions (14 wavelength band total, with 5 in the TIR and 6 in the SWIR). This multiscale spatial resolution across a wide wavelength range provides a unique tool for volcanological applications. For example, the wavelength range coupled with the variable gain settings allows the acquisition of unsaturated data over a wide temperature range (-73 – 1393 °C). Furthermore, saturation in one wavelength region (e.g., the TIR) can be compensated using the nested pixels from a shorter wavelength region (e.g., the 9 SWIR or 36 VNIR pixels) to correct for that saturation (e.g., [38]). These data enable thermal anomalies of only a few degrees above the background temperature, as well as sub-pixel, highly radiant anomalies of only several m^2 , to be determined.

For the past 15 years, an ASTER-focused program called the Urgent Request Protocol (URP) has combined the rapid detection capability of higher temporal resolution instruments like MODIS with the high spatial resolution scheduled observations of ASTER. These observations have improved our knowledge of multi-year volcanic monitoring, ongoing eruption behavior, and post-eruption change. They have also become important for capturing points-in-time during any ongoing lava flow or plume forming eruption. More commonly, the ASTER URP data (as well as the entire ASTER volcanic archive) are being used for operational response to new eruptions; determining thermal trends months prior to an eruption; inferring the emplacement of new lava lobes; and mapping the constituents of volcanic plumes, to name a few (see Appendix A). These all require the higher spatial resolution data of ASTER, and in most cases, its multispectral capability.

A framework like the URP sensor web only works in its current form if there is a large enough radiant target to be detected by the operational systems using MODIS data like MODVOLC and MIROVA. The MIROVA system applies an enhanced thermal index (ETI) and therefore detects more subtle thermal signals as compared to MODVOLC [32]. Even with this enhanced detection, however, there will be a significant number of thermal events and numerous volcanoes missed every year because they are not large enough (spatially or radiantly) to be detected in a 1 km MODIS pixel. It is

these smaller signals that are frequently important as they indicate the onset of renewed activity, sometimes months to years prior to an eruption [22].

There are some volcanoes whose eruptions are long-lived enough and/or whose character changes throughout their ongoing eruptions, which allow sporadic larger signals to be detected with MODIS. These then trigger subsequent ASTER data, which captures more subtle, transient activity. The best examples of such activity are typically dome-forming eruptions. Larger thermal signals are caused by dome collapse exposing the hotter material or periodic larger dome-destroying eruptions. With renewed dome growth, the cooler carapace insulates the hotter interior and limits detection by MODIS. One of the best examples of this eruptive style is Sheveluch volcano, Russia. In a recent set of three observations by ASTER over a one week period, small changes in the dome's thermal output and moderately sized block-and-ash flows were captured (Figure 9). Although interesting from a volcanological perspective for Sheveluch, it is these relatively high-frequency ASTER URP data, captured over the one to multi-year timeframe, which greatly improve our understanding of how eruptions proceed and how volcanoes reawaken.

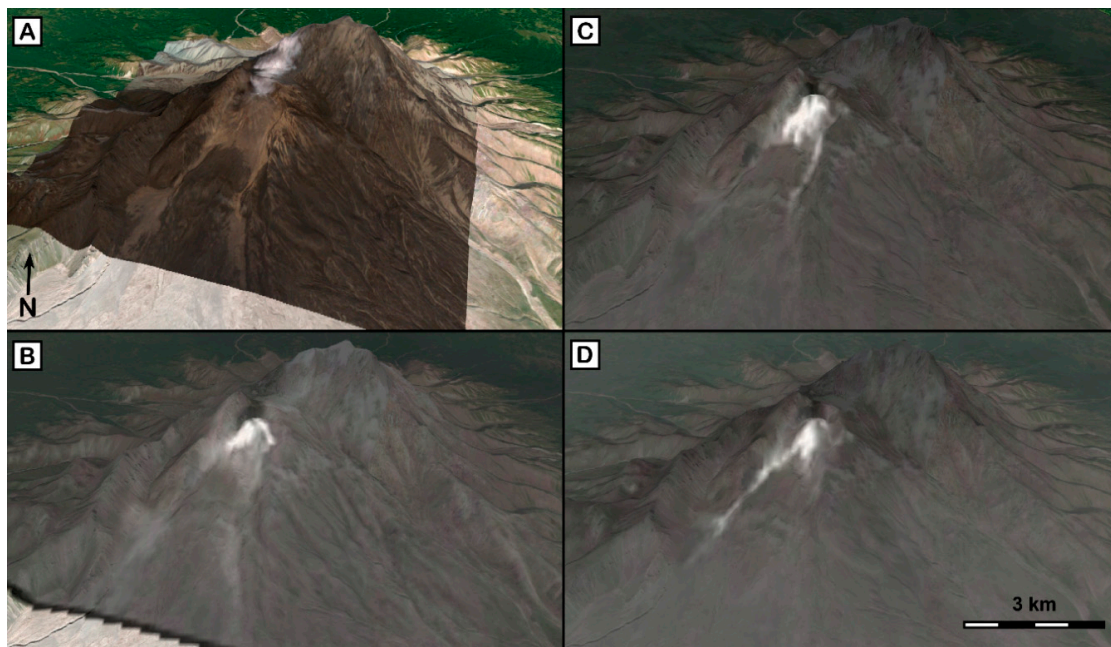


Figure 9. An example of the improved time series made possible by the ASTER URP Program, here showing the ASTER data draped over a 3D Google Earth visible image viewed looking NW toward Sheveluch volcano, Russia (summit location: 56.65°N, 161.36°E). (A) ASTER VNIR image acquired on 20 April 2019. The small white plume is visible drifting to the north. (B) ASTER TIR data from the same date. Two thermally elevated regions are seen on the summit lava dome. (C) ASTER nighttime TIR image acquired ~36 h later (21 April 2019) showing a significant increase in the area of the thermally elevated region on the dome and a ~2 km flow down the eastern side of the valley. (D) ASTER nighttime TIR data acquired on 28 April 2019 showing the continued, but somewhat lower, thermal activity on the dome and a new debris flow extending ~3 km down the western side of the valley.

6. Conclusions

Despite the two-decade archive of multispectral, multispatial resolution ASTER data (or perhaps because of its success), there have been no approved follow-on instruments by NASA or other space agencies that have similar spatial and spectral scales. Some of this land imaging is filled by sensors on the Landsat, Sentinel-2, and SPOT satellites, but the data gap discrepancy looms largest in the TIR. Currently, only the limited mission lifetime ECOSTRESS instrument on the ISS is the most similar. This gap was also noted in both the 2007 and 2018 Decadal Surveys for NASA Earth Science. In 2007, a notional mission called HypIRI was recommended, from which ECOSTRESS derives its heritage.

In 2018, the focus was on specific science questions and important designated observables. TIR data was again highlighted numerous times.

What will arise from the 2018 recommendations is yet to be formulated. TIR instruments will likely get smaller and more numerous using uncooled detectors, becoming CubeSat compatible and operating in a dense sensor web network for improved response times. Although perhaps not designed specifically for volcanology, the data from these instruments will become critical for volcanic crisis response and enable never before possible measurements such as the global inventory of volcanic degassing, thermal precursory trends at every volcano, and accurate temperatures of small activity, which can be used as input to predictive flow and hazard assessment models.

This next generation of high spatial, high spectral TIR data captured at ever-improving temporal resolutions will only become possible because of the ASTER instrument design and mission success, most notably for volcanic remote sensing. For example, with the Terra spacecraft's converging orbits at the poles, higher latitude volcanoes like those in Kamchatka, Iceland, and Antarctica are imaged more routinely. The addition of off-axis pointing in the ASTER design and the later establishment of the STAR and URP Programs further improved this temporal resolution to near the theoretical maximum. Multispectral TIR data are now being routinely acquired that allow us to track subtle thermal anomalies, precursory activity, explosive events, plumes, and the percentage of obscuring clouds. These data can help inform future instrument and mission design. For example, looking again at the data in Table 2, one can calculate a "miss rate percentage" between the number of MODIS-based triggers and the number of ASTER scenes acquired from those triggers. This rate varies from a low of 39.8% (Popocatepetl volcano) to a maximum of 96.2% (Erta Ale volcano), with an average of 87.6%. These high values demonstrate the amount of high spatial resolution data that are theoretically being missed because there is not a TIR sensor or sensor system with the spatial/spectral resolution of ASTER and the temporal resolution of MODIS. Perhaps even more critically, with an average cloud percentage near 50% based on our analysis of the ASTER URP archive, half of the current observation attempts fail to detect surface activity. This further highlights the need for improved temporal resolution. Ultimately, these results provide a baseline for future TIR orbital concepts that could respond to the 2018 Decadal Survey recommendations for the TIR data critically needed to address key science questions.

Author Contributions: The following contributions were provided by each author: conceptualization, M.S.R.; data curation, I.T.W.F. and M.S.R.; formal analysis, M.S.R. and I.T.W.F.; funding acquisition, M.S.R.; investigation, M.S.R. and I.T.W.F.; methodology, M.S.R.; project administration, M.S.R.; resources, M.S.R.; supervision, M.S.R.; validation, M.S.R. and I.T.W.F.; visualization, M.S.R.; writing—original draft, M.S.R.; writing—review and editing, M.S.R. and I.T.W.F. All authors have read and agreed to the published version of the manuscript.

Funding: This work was supported by NASA and several successful proposals to the Science of Terra and Aqua Program over the years, with the current being 80NSSC18K1001.

Acknowledgments: The authors wish to thank the members of the ASTER Science Team for helpful discussions, comments, and support during the past 20 years of the mission—in particular, David Pieri at the Jet Propulsion Laboratory, who, along with Minoru Urai at the Geologic Survey of Japan, headed up the early days of volcano science with ASTER. We would like to thank Ben McKeeby for his assistance with the ASTER archival search and creation of Figure 8, as well as Tyler Leggett, Marco Michelini, James Thompson, and Daniel Williams for their assistance with the painstaking reference checking for the Appendix A. We apologize in advance for any papers inadvertently left off this list; it was not intentional. We intend to keep this list updated on the lead author's laboratory website (<http://ivis.eps.pitt.edu/archives/ASTER/>). Please send any future or past/missing references to the lead author and they will be added to the online table. Finally, the authors would like to thank the three anonymous reviewers, whose comments and suggestions helped to improve the quality of this manuscript.

Conflicts of Interest: The authors declare no conflict of interest.

Appendix A

Table A1. Reference list of 271 volcanological publications that use, contain, or make mention of (in the case of the Precursory category) ASTER data. The list spans 25 years, from 1995 to 2019, and is subdivided by category with references therein listed in chronological order. The full citations appear below.

Publication Category	Reference List
Analogs	Davies et al., 2008; Price et al., 2016; Ramsey et al., 2016.
Calibration	Barreto et al., 2010; Vaughan et al., 2010; Blackett & Wooster, 2011; Thompson et al., 2019.
Gas/Plumes	Corradini et al., 2003; Urai, 2003; Urai, 2004; Ino et al., 2005; Iwashita et al., 2006; Pugnaghi et al., 2006; Kearney et al., 2008; Campion et al., 2010; Diaz et al., 2010; Kobayashi et al., 2010b; Camiz et al., 2010; Spinetti et al., 2011; Campion et al., 2012; Henney et al., 2012; Abrams et al., 2013; Pieri et al., 2013; Spinetti et al., 2013; Campion, 2014; Diaz et al., 2015; Stebel et al., 2015; Carn et al., 2016; Realmuto & Berk, 2016; Robertson et al., 2016; Xi et al., 2016; Kern et al., 2017; Moussallam et al., 2017; Troncoso et al., 2017; Williams & Ramsey, 2019; Williams et al., 2019; Laiolo et al., 2019.
Geothermal	Hellman & Ramsey, 2004; Viramonte et al., 2005; Vaughan et al., 2012a; Vaughan et al., 2012b; Silvestri et al., 2016; Braddock et al., 2017; Caudron et al., 2018; Mia et al., 2018a; Mia et al., 2018b.
Lava Flows	Wright et al., 2010; Favalli et al., 2012; Wadge et al., 2012; Head et al., 2013.
Mapping	Hubbard et al., 2003; Rowan et al., 2003; Watanabe & Matsue, 2003; Byrnes et al., 2004; Torres et al., 2004; Dmochowski, 2005; Tralli et al., 2005; Capra, 2006; Mars & Rowan, 2005; Rowan et al., 2006; Coolbaugh et al., 2007; Davila et al., 2007; Hubbard et al., 2007; Kervyn et al., 2007; Carter et al., 2008; Kervyn et al., 2008c; Saepuloh et al., 2008; Schneider et al., 2008; Carter & Ramsey, 2009; Baliatan & Obille, 2009; Bogie et al., 2010; Brandmeier, 2010; Kobayashi et al., 2010a; Piscini et al., 2010; Chadwick et al., 2011; Davila-Hernandez et al., 2011; Mars & Rowan, 2011; Wadge & Burt, 2011; Wantim et al., 2011; Diaz-Castellon et al., 2012; Amici et al., 2013; Graettinger et al., 2013; Lara et al., 2013; Watt et al., 2013; Boyce et al., 2014; Mars, 2014; Tayebi et al., 2014; Castruccia & Clavero, 2015; Ramsey, 2015; Selles et al., 2015; Folguera et al., 2016; Oikonomidis et al., 2016; Prambada et al., 2016; Suminar et al., 2016; Ulusoy, 2016; Yulianto & Sofan, 2016; Ali-Bik et al., 2017; Bustos et al., 2017; Takarada, 2017; Auer et al., 2018; Godoy et al., 2018; Krippner et al., 2018; Aufaristama et al., 2019b; Fu et al., 2019; Pallister et al., 2019.
Modeling	Favalli et al., 2006; Huggel et al., 2007; Huggel et al., 2008; Carter et al., 2009; Favalli et al., 2009; Joyce et al., 2009b; Munoz-Salinas et al., 2009; Capra et al., 2011; Sosio et al., 2012; Worni et al., 2012; Wantim et al., 2013; Rose et al., 2014; Rose & Ramsey, 2015; Carr et al., 2019; Ramsey et al., 2019; Rogic et al., 2019.
Monitoring	Tsu et al., 2001; Urai et al., 2001; Ellrod et al., 2002; Mattiolo et al., 2004; Pieri & Abrams, 2004; Ramsey & Flynn, 2004; Ramsey & Dehn, 2004; Patrick et al., 2005; Pieri & Abrams, 2005; Wright et al., 2005; Gogu et al., 2006; Vaughan & Hook, 2006; Carter et al., 2007; Permenter & Oppenheimer, 2007; Vaughan et al., 2007; Hirn et al., 2008; Joyce et al., 2008; Kervyn et al., 2008b; Moran et al., 2008; Sincioco, 2008; Tunk & Bernard, 2008; Vaughan et al., 2008; Ji et al., 2009; Joyce et al., 2009a; Rose & Ramsey, 2009; Zlotnicki et al., 2009; Bailey et al., 2010; Carter & Ramsey, 2010; Coombs et al., 2010; Ferguson et al., 2010; Ganas et al., 2010; Ji et al., 2010; Murphy et al., 2010; Thomas & Watson, 2010; Wessels et al., 2010; Urai & Pieri, 2010; Grishin, 2011; Mathieu et al., 2011; Murphy et al., 2011; Rybin et al., 2011; Saepuloh et al., 2011; Urai, 2011; Urai & Ishizuka, 2011; Gutierrez et al., 2012; Hooper et al., 2012; Jousset et al., 2012; Patrick & Orr, 2012; Ramsey et al., 2012; Solikhin et al., 2012; Bleick et al., 2013; Buongiorno et al., 2013; Colvin et al., 2013; Dvigalo et al., 2013; Girina, 2013; Jay et al., 2013; Murphy et al., 2013; Ramsey & Harris, 2013; Roverato et al., 2013; Saepuloh et al., 2013; Wessels et al., 2013; West, 2013; Delgado et al., 2014; McGimsey et al., 2014; Moyano et al., 2014; Pritchard et al., 2014; Smets et al., 2014; Worden et al., 2014; Jay et al., 2015; Mars et al., 2015; Volynets et al., 2015; Whelley et al., 2015; Brothelande et al., 2016; Carr et al., 2016; Naranjo et al., 2016; Patrick et al., 2016; Rathnam & Ramashri, 2016a; Rathnam & Ramashri, 2016b; Reath et al., 2016; Blackett, 2017; Furtney et al., 2018; Girina et al., 2018; Girona et al., 2018; Harris et al., 2018; Plank et al., 2018; Wadge et al., 2018; Aufaristama et al., 2019a; Caputo et al., 2019; Gray et al., 2019; Harris et al., 2019; Henderson et al., 2019; Kaneko et al., 2019; Mannini et al., 2019; Mia et al., 2019; Reath et al., 2019; Sekertekin & Arslan, 2019; Silvestri et al., 2019.
Operational	Duda et al., 2009; Patrick & Witzke, 2011; Abrams et al., 2015; Ramsey, 2016.
Other	Scholte et al., 2003; Patrick et al., 2004; Mantas et al., 2011; Rivera et al., 2014.

Table A1. Cont.

Publication Category	Reference List
Precursory	Fujisada, 1995; Pieri et al., 1995; Oppenheimer, 1996; Oppenheimer, 1997; Realmuto et al., 1997; Oppenheimer et al., 1998; Yamaguchi et al., 1998; Glaze et al., 1999; Harris et al., 1999; Ramsey & Fink, 1999; Urai et al., 1999; Wright et al., 1999; Flynn et al., 2000; Realmuto, 2000; Realmuto & Worden, 2000; Wright et al., 2000.
Topography	Stevens et al., 2004; Kass, 2005; Kervyn et al., 2006; Pavez et al., 2006; Urai et al., 2007; Kervyn et al., 2008a; Arellano-Baeza et al., 2009; Gilichinsky et al., 2010; Inbar et al., 2011; Volker et al., 2011; Zouzias et al., 2011; Ebmeier et al., 2012; Fornaciai et al., 2012; Grosse et al., 2012; Camiz et al., 2013; Ebmeier et al., 2013; Le Corvec et al., 2013; Pritchard et al., 2013; Hamlyn et al., 2013; Kim & Lees, 2014; Albino et al., 2015; Walter et al., 2015; Kereszturi & Procter, 2016; Bannari et al., 2017; Camiz et al., 2017; Girod et al., 2017; Holohan et al., 2017; Aisyah et al., 2018; Raharimahefa & Rasoazanamparany, 2018; Deng et al., 2019; Morgado et al., 2019.

Complete Reference List for Table A1.

- Abrams, M.; Pieri, D.; Realmuto, V.; Wright, R. Using EO-1 Hyperion Data as HypsIRI Preparatory Data Sets for Volcanology Applied to Mt Etna, Italy. *IEEE J. Sel. Top. Appl. Earth Obs. Remote Sens.* **2013**, *6* (2), 375–385. <https://doi.org/10.1109/JSTARS.2012.2224095>.
- Abrams, M.; Tsu, H.; Hulley, G.; Iwao, K.; Pieri, D.; Cudahy, T.; Kargel, J. The Advanced Spaceborne Thermal Emission and Reflection Radiometer (ASTER) after Fifteen Years: Review of Global Products. *Int. J. Appl. Earth Obs. Geoinf.* **2015**, *38*, 292–301. <https://doi.org/10.1016/j.jag.2015.01.013>.
- Aisyah, N.; Iguchi, M.; Subandriyo; Budisantoso, A.; Hotta, K.; Sumarti, S. Combination of a Pressure Source and Block Movement for Ground Deformation Analysis at Merapi Volcano Prior to the Eruptions in 2006 and 2010. *J. Volcanol. Geotherm. Res.* **2018**, *357*, 239–253. <https://doi.org/10.1016/j.jvolgeores.2018.05.001>.
- Albino, F.; Smets, B.; D'Oreye, N.; Kervyn, F. High-Resolution TanDEM-X DEM: An Accurate Method to Estimate Lava Flow Volumes at Nyamulagira Volcano (D. R. Congo). *J. Geophys. Res. Solid Earth.* **2015**, *120* (6), 4189–4207. <https://doi.org/10.1002/2015JB011988>.
- Ali-Bik, M. W.; Abd El Rahim, S. H.; Wahab, W. A.; Abayazeed, S. D.; Hassan, S. M. Geochemical Constraints on the Oldest Arc Rocks of the Arabian-Nubian Shield: The Late Mesoproterozoic to Late Neoproterozoic (?) Sa'al Volcano-Sedimentary Complex, Sinai, Egypt. *Lithos.* **2017**, *284–285*, 310–326. <https://doi.org/10.1016/j.lithos.2017.03.031>.
- Amici, S.; Piscini, A.; Buongiorno, M. F.; Pieri, D. Geological Classification of Volcano Teide by Hyperspectral and Multispectral Satellite Data. *Int. J. Remote Sens.* **2013**, *34* (9–10), 3356–3375. <https://doi.org/10.1080/01431161.2012.716913>.
- Arellano-Baeza, A. A.; García, R. V.; Trejo-Soto, M.; Martínez Bringas, A. Use of the ASTER Satellite Images for Evaluation of Structural Changes in the Popocatepetl Volcano Related to Microseismicity. *Adv. Sp. Res.* **2009**, *43* (2), 224–230. <https://doi.org/10.1016/j.asr.2008.03.021>.
- Auer, A.; Belousov, A.; Belousova, M. Deposits, Petrology and Mechanism of the 2010–2013 Eruption of Kizimen Volcano in Kamchatka, Russia. *Bull. Volcanol.* **2018**, *80* (4), 4. <https://doi.org/10.1007/s00445-018-1199-z>.
- Aufaristama, M.; Hoskuldsson, A.; Jonsdottir, I.; Ulfarsson, M. O.; Erlangga, I. G. D.; Thordarson, T. Thermal Model of Lava in Mt. Agung during December 2017 Episodes Derived from Integrated SENTINEL 2A and ASTER Remote Sensing Datasets. In *IOP Conference Series: Earth and Environmental Science*; 2019a; Vol. 311, p 1. <https://doi.org/10.1088/1755-1315/311/1/012016>.
- Aufaristama, M.; Hoskuldsson, A.; Ulfarsson, M. O.; Jonsdottir, I.; Thordarson, T. The 2014–2015 Lava Flow Field at Holuhraun, Iceland: Using Airborne Hyperspectral Remote Sensing for Discriminating the Lava Surface. *Remote Sens.* **2019b**, *11* (5), 5. <https://doi.org/10.3390/rs11050476>.
- Bailey, J. E.; Dean, K. G.; Dehn, J.; Webley, P. W. Integrated Satellite Observations of the 2006 Eruption of Augustine Volcano. *US Geol. Surv. Prof. Pap.* **2010**, No. 1769, 481–503. <https://doi.org/10.3133/pp176920>.

- Bannari, A.; Kadhem, G.; Hameid, N.; El-Battay, A. Small Islands DEMs and Topographic Attributes Analysis: A Comparative Study among SRTM-V4.1, ASTER-V2.1, High Topographic Contours Map and DGPS. *J. Earth Sci. Eng.* **2017**, *7* (2), 90–119. <https://doi.org/10.17265/2159-581x/2017.02.003>.
- Barreto, Á.; Arbelo, M.; Hernández-Leal, P. A.; Núñez-Casillas, L.; Mira, M.; Coll, C. Evaluation of Surface Temperature and Emissivity Derived from ASTER Data: A Case Study Using Ground-Based Measurements at a Volcanic Site. *J. Atmos. Ocean. Technol.* **2010**, *27* (10), 1677–1688. <https://doi.org/10.1175/2010JTECHA1447.1>.
- Blackett, M. An Overview of Infrared Remote Sensing of Volcanic Activity. *J. Imaging* **2017**, *3* (2). <https://doi.org/10.3390/jimaging3020013>.
- Blackett, M.; Wooster, M. J. Evaluation of SWIR-Based Methods for Quantifying Active Volcano Radiant Emissions Using NASA EOS-ASTER Data. *Geomatics, Nat. Hazards Risk.* **2011**, *2* (1), 51–78. <https://doi.org/10.1080/19475705.2010.541501>.
- Bleick, H. A.; Coombs, M. L.; Cervelli, P. F.; Bull, K. F.; Wessels, R. L. Volcano-Ice Interactions Precursory to the 2009 Eruption of Redoubt Volcano, Alaska. *J. Volcanol. Geotherm. Res.* **2013**, *259*, 373–388. <https://doi.org/10.1016/j.jvolgeores.2012.10.008>.
- Bogie, I.; Sugiono, S. R.; Malike, D. Volcanic Landforms That Mark the Successfully Developed Geothermal Systems of Java, Indonesia Identified from ASTER Satellite Imagery. In *Proceedings World Geothermal Congress*, 2010; pp1-9.
- Boyce, J. A.; Keays, R. R.; Nicholls, I. A.; Hayman, P. Eruption Centres of the Hamilton Area of the Newer Volcanics Province, Victoria, Australia: Pinpointing Volcanoes from a Multifaceted Approach to Landform Mapping. *Aust. J. Earth Sci.* **2014**, *61* (5), 735–754. <https://doi.org/10.1080/08120099.2014.923508>.
- Braddock, M.; Biggs, J.; Watson, I. M.; Hutchison, W.; Pyle, D. M.; Mather, T. A. Satellite Observations of Fumarole Activity at Aluto Volcano, Ethiopia: Implications for Geothermal Monitoring and Volcanic Hazard. *J. Volcanol. Geotherm. Res.* **2017**, *341*, 70–83. <https://doi.org/10.1016/j.jvolgeores.2017.05.006>.
- Brandmeier, M. Remote Sensing of Carhuarazo Volcanic Complex Using ASTER Imagery in Southern Peru to Detect Alteration Zones and Volcanic Structures - a Combined Approach of Image Processing in ENVI and ArcGIS/ArcScene. *Geocarto Int.* **2010**, *25* (8), 629–648. <https://doi.org/10.1080/10106049.2010.519787>.
- Brothelande, E.; Lénat, J. F.; Chaput, M.; Gailler, L.; Finizola, A.; Dumont, S.; Peltier, A.; Bachèlery, P.; Barde-Cabusson, S.; Byrdina, S.; et al. Structure and Evolution of an Active Resurgent Dome Evidenced by Geophysical Investigations: The Yenkahe Dome-Yasur Volcano System (Siwi Caldera, Vanuatu). *J. Volcanol. Geotherm. Res.* **2016**, *322*, 241–262. <https://doi.org/10.1016/j.jvolgeores.2015.08.021>.
- Buongiorno, M. F.; Pieri, D.; Silvestri, M. Thermal Analysis of Volcanoes Based on 10 Years of ASTER Data on Mt. Etna. In *Thermal Infrared Remote Sensing: Sensors, Methods, Applications*; Kuenzer, C., Dech, S., Eds.; Springer Netherlands: Dordrecht, **2013**; pp 409–428. https://doi.org/10.1007/978-94-007-6639-6_20.C.
- Bustos, E.; Báez, W. A.; Chiodi, A. L.; Arnosio, J. M.; Norini, G.; Groppell, G. Using Optical Imagery Data for Lithological Mapping of Composite Volcanoes in High Arid Puna Plateau. Tuzgle Volcano Case Study. *Rev. la Asoc. Geol. Argentina.* **2017**, *74* (3), 357–371.
- Byrnes, J. M.; Ramsey, M. S.; Crown, D. A. Surface Unit Characterization of the Mauna Ulu Flow Field, Kilauea Volcano, Hawai'i, Using Integrated Field and Remote Sensing Analyses. *J. Volcanol. Geotherm. Res.* **2004**, *135* (1–2), 169–193. <https://doi.org/10.1016/j.jvolgeores.2003.12.016>.
- Camiz, S.; Poscolieri, M.; Roverato, M. Comparison of Three Andean Volcanic Complexes through Multidimensional Analyses of Geomorphometric Data. *G. Bianchini al., EICES.* **2013**, 52–74.
- Camiz, S.; Poscolieri, M.; Roverato, M. Geomorphometric Comparative Analysis of Latin-American Volcanoes. *J. South Am. Earth Sci.* **2017**, *76*, 47–62. <https://doi.org/10.1016/j.jsames.2017.02.011>.
- Campion, R. New Lava Lake at Nyamuragira Volcano Revealed by Combined ASTER and OMI SO₂ Measurements. *Geophys. Res. Lett.* **2014**, *41* (21), 7485–7492. <https://doi.org/10.1002/2014GL061808>.

- Campion, R.; Salerno, G. G.; Coheur, P. F.; Hurtmans, D.; Clarisse, L.; Kazahaya, K.; Burton, M.; Caltabiano, T.; Clerbaux, C.; Bernard, A. Measuring Volcanic Degassing of SO₂ in the Lower Troposphere with ASTER Band Ratios. *J. Volcanol. Geotherm. Res.* **2010**, *194* (1–3), 42–54. <https://doi.org/10.1016/j.jvolgeores.2010.04.010>.
- Campion, R.; Martinez-Cruz, M.; Lecocq, T.; Caudron, C.; Pacheco, J.; Pinardi, G.; Hermans, C.; Carn, S.; Bernard, A. Space- and Ground-Based Measurements of Sulphur Dioxide Emissions from Turrialba Volcano (Costa Rica). *Bull. Volcanol.* **2012**, *74* (7), 1757–1770. <https://doi.org/10.1007/s00445-012-0631-z>.
- Capra, L. Volcanic Natural Dams Associated with Sector Collapses: Textural and Sedimentological Constraints on Their Stability. *Ital. J. Eng. Geol. Environ.* **2006**, *2006*, 279–294. https://doi.org/10.1007/978-3-642-04764-0_9.
- Capra, L.; Manea, V. C.; Manea, M.; Norini, G. The Importance of Digital Elevation Model Resolution on Granular Flow Simulations: A Test Case for Colima Volcano Using TITAN2D Computational Routine. *Nat. Hazards* **2011**, *59* (2), 665–680. <https://doi.org/10.1007/s11069-011-9788-6>.
- Caputo, T.; Sessa, E. B.; Silvestri, M.; Buongiorno, M. F.; Musacchio, M.; Sansivero, F.; Vilardo, G. Surface Temperature Multiscale Monitoring by Thermal Infrared Satellite and Ground Images at Campi Flegrei Volcanic Area (Italy). *Remote Sens.* **2019**, *11* (9), 1007. <https://doi.org/10.3390/rs11091007>.
- Carn, S. A.; Clarisse, L.; Prata, A. J. Multi-Decadal Satellite Measurements of Global Volcanic Degassing. *J. Volcanol. Geotherm. Res.* **2016**, *311*, 99–134. <https://doi.org/10.1016/j.jvolgeores.2016.01.002>.
- Carr, B. B.; Clarke, A. B.; Vanderkluyzen, L. The 2006 Lava Dome Eruption of Merapi Volcano (Indonesia): Detailed Analysis Using MODIS TIR. *J. Volcanol. Geotherm. Res.* **2016**, *311*, 60–71. <https://doi.org/10.1016/j.jvolgeores.2015.12.004>.
- Carr, B. B.; Clarke, A. B.; Vanderkluyzen, L.; Arrowsmith, J. R. Mechanisms of Lava Flow Emplacement during an Effusive Eruption of Sinabung Volcano (Sumatra, Indonesia). *J. Volcanol. Geotherm. Res.* **2019**, *382*, 137–148. <https://doi.org/10.1016/j.jvolgeores.2018.03.002>.
- Carter, A. J.; Ramsey, M. S. ASTER- and Field-Based Observations at Bezymianny Volcano: Focus on the 11 May 2007 Pyroclastic Flow Deposit. *Remote Sens. Environ.* **2009**, *113* (10), 2142–2151. <https://doi.org/10.1016/j.rse.2009.05.020>.
- Carter, A.; Ramsey, M. S. Long-Term Volcanic Activity at Shiveluch Volcano: Nine Years of ASTER Spaceborne Thermal Infrared Observations. *Remote Sens.* **2010**, *2* (11), 2571–2583. <https://doi.org/10.3390/rs2112571>.
- Carter, A. J.; Ramsey, M. S.; Belousov, A. B. Detection of a New Summit Crater on Bezymianny Volcano Lava Dome: Satellite and Field-Based Thermal Data. *Bull. Volcanol.* **2007**, *69* (7), 811–815. <https://doi.org/10.1007/s00445-007-0113-x>.
- Carter, A. J.; Girina, O.; Ramsey, M. S.; Demyanchuk, Y. V. ASTER and Field Observations of the 24 December 2006 Eruption of Bezymianny Volcano, Russia. *Remote Sens. Environ.* **2008**, *112* (5), 2569–2577. <https://doi.org/10.1016/j.rse.2007.12.001>.
- Carter, A. J.; Ramsey, M. S.; Durant, A. J.; Skilling, I. P.; Wolfe, A. Micron-Scale Roughness of Volcanic Surfaces from Thermal Infrared Spectroscopy and Scanning Electron Microscopy. *J. Geophys. Res. Solid Earth.* **2009**, *114* (2), 13. <https://doi.org/10.1029/2008JB005632>.
- Castruccio, A.; Clavero, J. Lahar Simulation at Active Volcanoes of the Southern Andes: Implications for Hazard Assessment. *Nat. Hazards* **2015**, *77* (2), 693–716. <https://doi.org/10.1007/s11069-015-1617-x>.
- Caudron, C.; Bernard, A.; Murphy, S.; Inguaggiato, S.; Gunawan, H. Volcano-Hydrothermal System and Activity of Sirung Volcano (Pantar Island, Indonesia). *J. Volcanol. Geotherm. Res.* **2018**, *357*, 186–199. <https://doi.org/10.1016/j.jvolgeores.2018.04.011>.
- Chadwick, W. W.; Jónsson, S.; Geist, D. J.; Poland, M.; Johnson, D. J.; Batt, S.; Harpp, K. S.; Ruiz, A. The May 2005 Eruption of Fernandina Volcano, Galápagos: The First Circumferential Dike Intrusion Observed by GPS and InSAR. *Bull. Volcanol.* **2011**, *73* (6), 679–697. <https://doi.org/10.1007/s00445-010-0433-0>.

- Colvin, A.; Rose, W. I.; Varekamp, J. C.; Palma, J. L.; Escobar, D.; Gutierrez, E.; Montalvo, F.; Maclean, A. Crater Lake Evolution at Santa Ana Volcano (El Salvador) Following the 2005 Eruption. *Spec. Pap. Geol. Soc. Am.* **2013**, *498*, 23–43. [https://doi.org/10.1130/2013.2498\(02\)](https://doi.org/10.1130/2013.2498(02)).
- Coolbaugh, M. F.; Kratt, C.; Fallacaro, A.; Calvin, W. M.; Taranik, J. V. Detection of Geothermal Anomalies Using Advanced Spaceborne Thermal Emission and Reflection Radiometer (ASTER) Thermal Infrared Images at Bradys Hot Springs, Nevada, USA. *Remote Sens. Environ.* **2007**, *106* (3), 350–359. <https://doi.org/10.1016/j.rse.2006.09.001>.
- Coombs, M. L.; Bull, K. F.; Vallance, J. W.; Schneider, D. J.; Thoms, E. E.; Wessels, R. L.; McGimsey, R. G. Timing, Distribution, and Volume of Proximal Products of the 2006 Eruption of Augustine Volcano. *US Geol. Surv. Prof. Pap.* **2010**, No. 1769, 145–185.
- Coppola, D.; Champion, R.; Laiolo, M.; Cuoco, E.; Balagizi, C.; Ripepe, M.; Cigolini, C.; Tedesco, D. Birth of a Lava Lake: Nyamulagira Volcano 2011–2015. *Bull. Volcanol.* **2016**, *78* (3), 1–13. <https://doi.org/10.1007/s00445-016-1014-7>.
- Corradini, S.; Pugnaghi, S.; Teggi, S.; Buongiorno, M. F.; Bogliolo, M. P. Will ASTER See the Etna SO₂ Plume? *Int. J. Remote Sens.* **2003**, *24* (6), 1207–1218. <https://doi.org/10.1080/01431160210153084>.
- Davies, A. G.; Calkins, J.; Scharenbroich, L.; Vaughan, R. G.; Wright, R.; Kyle, P.; Castaño, R.; Chien, S.; Tran, D. Multi-Instrument Remote and in Situ Observations of the Erebus Volcano (Antarctica) Lava Lake in 2005: A Comparison with the Pele Lava Lake on the Jovian Moon Io. *J. Volcanol. Geotherm. Res.* **2008**, *177* (3), 705–724. <https://doi.org/10.1016/j.jvolgeores.2008.02.010>.
- Davila, N.; Capra, L.; Gavilanes-Ruiz, J. C.; Varley, N.; Norini, G.; Vazquez, A. G. Recent Lahars at Volcán de Colima (Mexico): Drainage Variation and Spectral Classification. *J. Volcanol. Geotherm. Res.* **2007**, *165* (3–4), 127–141. <https://doi.org/10.1016/j.jvolgeores.2007.05.016>.
- Dávila-Hernández, N.; Lira, J.; Capra-Pedol, L.; Zucca, F. A Normalized Difference Lahar Index Based on Terra/Aster and Spot 5 Images: An Application at Colima Volcano, Mexico. *Rev. Mex. Ciencias Geol.* **2011**, *28* (3), 630–644.
- Delgado, F.; Pritchard, M.; Lohman, R.; Naranjo, J. A. The 2011 Hudson Volcano Eruption (Southern Andes, Chile): Pre-Eruptive Inflation and Hotspots Observed with InSAR and Thermal Imagery. *Bull. Volcanol.* **2014**, *76* (5), 1–19. <https://doi.org/10.1007/s00445-014-0815-9>.
- Deng, F.; Rodgers, M.; Xie, S.; Dixon, T. H.; Charbonnier, S.; Gallant, E. A.; López Vélez, C. M.; Ordoñez, M.; Malservisi, R.; Voss, N. K.; et al. High-Resolution DEM Generation from Spaceborne and Terrestrial Remote Sensing Data for Improved Volcano Hazard Assessment — A Case Study at Nevado Del Ruiz, Colombia. *Remote Sens. Environ.* **2019**, *233*, 11134. <https://doi.org/10.1016/j.rse.2019.111348>.
- Diaz, J. A.; Pieri, D.; Arkin, C. R.; Gore, E.; Griffin, T. P.; Fladeland, M.; Bland, G.; Soto, C.; Madrigal, Y.; Castillo, D.; et al. Utilization of in Situ Airborne MS-Based Instrumentation for the Study of Gaseous Emissions at Active Volcanoes. *Int. J. Mass Spectrom.* **2010**, *295* (3), 105–112. <https://doi.org/10.1016/j.ijms.2010.04.013>.
- Diaz, J. A.; Pieri, D.; Wright, K.; Sorensen, P.; Kline-Shoder, R.; Arkin, C. R.; Fladeland, M.; Bland, G.; Buongiorno, M. F.; Ramirez, C.; et al. Unmanned Aerial Mass Spectrometer Systems for In-Situ Volcanic Plume Analysis. *J. Am. Soc. Mass Spectrom.* **2015**, *26* (2), 292–304. <https://doi.org/10.1007/s13361-014-1058-x>.
- Díaz-Castellón, R.; Hubbard, B. E.; Carrasco-Núñez, G.; Rodríguez-Vargas, J. L. The Origins of Late Quaternary Debris Avalanche and Debris Flow Deposits from Cofre de Perote Volcano, México. *Geosphere.* **2012**, *8* (4), 950–971. <https://doi.org/10.1130/GES00709.1>.
- Duba, K.A.; Ramsey, M.; Wessels, R.; Dehn, J. Optical Satellite Volcano Monitoring: A Multi-Sensor Rapid Response System. In *Geoscience and Remote Sensing*; 2009; pp 473–496. <https://doi.org/10.5772/8303>.
- Dvigalo, V. N.; Melekestsev, I. V.; Shevchenko, A. V.; Svirid, I. Y. The 2010–2012 Eruption of Kizimen Volcano: The Greatest Output (from the Data of Remote-Sensing Observations) for Eruptions in Kamchatka in the Early 21st Century Part I. The November 11, 2010 to December 11, 2011 Phase. *J. Volcanol. Seismol.* **2013**, *7* (6), 345–361. <https://doi.org/10.1134/S074204631306002X>.

- Ebmeier, S. K.; Biggs, J.; Mather, T. A.; Elliott, J. R.; Wadge, G.; Amelung, F. Measuring Large Topographic Change with InSAR: Lava Thicknesses, Extrusion Rate and Subsidence Rate at Santiaguito Volcano, Guatemala. *Earth Planet. Sci. Lett.* **2012**, *335–336*, 216–225. <https://doi.org/10.1016/j.epsl.2012.04.027>.
- Ebmeier, S. K.; Biggs, J.; Mather, T. A.; Amelung, F. Applicability of InSAR to Tropical Volcanoes: Insights from Central America. *Geol. Soc. Spec. Publ.* **2013**, *380* (1), 15–37. <https://doi.org/10.1144/SP380.2>.
- Ellrod, G. P.; Helz, R. L.; Wadge, G. *Volcanic Hazards Assessment*; CEOS. NOAA. gov, 2002.
- Favalli, M.; Chirico, G. D.; Papale, P.; Pareschi, M. T.; Coltelli, M.; Lucaya, N.; Boschi, E. Computer Simulations of Lava Flow Paths in the Town of Goma, Nyiragongo Volcano, Democratic Republic of Congo. *J. Geophys. Res. Solid Earth.* **2006**, *111* (6). <https://doi.org/10.1029/2004JB003527>.
- Favalli, M.; Chirico, G. D.; Papale, P.; Pareschi, M. T.; Boschi, E. Lava Flow Hazard at Nyiragongo Volcano, D.R.C. 1. Model Calibration and Hazard Mapping. *Bull. Volcanol.* **2009**, *71* (4), 363–374. <https://doi.org/10.1007/s00445-008-0233-y>.
- Favalli, M.; Tarquini, S.; Papale, P.; Fornaciai, A.; Boschi, E. Lava Flow Hazard and Risk at Mt. Cameroon Volcano. *Bull. Volcanol.* **2012**, *74* (2), 423–439. <https://doi.org/10.1007/s00445-011-0540-6>.
- Ferguson, D. J.; Barnie, T. D.; Pyle, D. M.; Oppenheimer, C.; Yirgu, G.; Lewi, E.; Kidane, T.; Carn, S.; Hamling, I. Recent Rift-Related Volcanism in Afar, Ethiopia. *Earth Planet. Sci. Lett.* **2010**, *292* (3–4), 409–418.
- Flynn, L. P.; Harris, A. J. L.; Rothery, D. A.; Oppenheimer, C. High-Spatial-Resolution Thermal Remote Sensing of Active Volcanic Features Using Landsat and Hyperspectral Data. *Geophys. Monogr. Ser.* **2000**, *116*, 161–177. <https://doi.org/10.1029/GM116p0161>.
- Folguera, A.; Rojas Vera, E.; Vélez, L.; Tobal, J.; Orts, D.; Agosto, M.; Caselli, A.; Ramos, V. A. A Review of the Geology, Structural Controls, and Tectonic Setting of Copahue Volcano, Southern Volcanic Zone, Andes, Argentina. In *Copahue Volcano*; Springer: Berlin, 2016; pp 3–22. https://doi.org/10.1007/978-3-662-48005-2_1.
- Fornaciai, A.; Favalli, M.; Karátson, D.; Tarquini, S.; Boschi, E. Morphometry of Scoria Cones, and Their Relation to Geodynamic Setting: A DEM-Based Analysis. *J. Volcanol. Geotherm. Res.* **2012**, *217–218*, 56–72. <https://doi.org/10.1016/j.jvolgeores.2011.12.012>.
- Fu, H.; Fu, B.; Ninomiya, Y.; Shi, P. New Insights of Geomorphologic and Lithologic Features Onwudalianchi Volcanoes in the Northeastern China from the ASTER Multispectral Data. *Remote Sens.* **2019**, *11* (22), 2663. <https://doi.org/10.3390/rs11222663>.
- Fujisada, H. Design and Performance of ASTER Instrument. Proceedings of SPIE. *Int. Soc. Opt. Eng.* **1995**, *2583* (2583), Int. Soc. Opt. Eng.
- Furtney, M. A.; Pritchard, M. E.; Biggs, J.; Carn, S. A.; Ebmeier, S. K.; Jay, J. A.; McCormick Kilbride, B. T.; Reath, K. A. Synthesizing Multi-Sensor, Multi-Satellite, Multi-Decadal Datasets for Global Volcano Monitoring. *J. Volcanol. Geotherm. Res.* **2018**, *365*, 38–56. <https://doi.org/10.1016/j.jvolgeores.2018.10.002>.
- Ganas, A.; Lagios, E.; Petropoulos, G.; Psiloglou, B. Thermal Imaging of Nisyros Volcano (Aegean Sea) Using ASTER Data: Estimation of Radiative Heat Flux. *Int. J. Remote Sens.* **2010**, *31* (15), 4033–4047. <https://doi.org/10.1080/01431160903140837>.
- Gilichinsky, M.; Melnikov, D.; Melekestsev, I.; Zaretskaya, N.; Inbar, M. Morphometric Measurements of Cinder Cones from Digital Elevation Models of Tolbachik Volcanic Field, Central Kamchatka. *Can. J. Remote Sens.* **2010**, *36* (4), 287–300. <https://doi.org/10.5589/m10-049>.
- Girina, O. A. Chronology of Bezymianny Volcano Activity, 1956–2010. *J. Volcanol. Geotherm. Res.* **2013**, *263*, 22–41. <https://doi.org/10.1016/j.jvolgeores.2013.05.002>.
- Girina, O. A.; Loupian, E. A.; Sorokin, A. A.; Mel’Nikov, D. V.; Manevich, A. G.; Manevich, T. M. Satellite and Ground-Based Observations of Explosive Eruptions on Zhupanovsky Volcano, Kamchatka, Russia in 2013 and in 2014–2016. *J. Volcanol. Seismol.* **2018**, *12* (1), 1–15. <https://doi.org/10.1134/S0742046318010049>.
- Girod, L.; Nuth, C.; Kääh, A.; McNabb, R.; Galland, O. MMASTER: Improved ASTER DEMs for Elevation Change Monitoring. *Remote Sens.* **2017**, *9* (7), 704. <https://doi.org/10.3390/rs9070704>.

- Girona, T.; Huber, C.; Caudron, C. Sensitivity to Lunar Cycles Prior to the 2007 Eruption of Ruapehu Volcano /704/4111 /704/2151/598 /141 Article. *Sci. Rep.* **2018**, *8* (1), 1476. <https://doi.org/10.1038/s41598-018-19307-z>.
- Glaze, L. S.; Wilson, L.; Mouginiis-Mark, P. J. Volcanic Eruption Plume Top Topography and Heights as Determined from Photoclinometric Analysis of Satellite Data. *J. Geophys. Res. Solid Earth.* **1999**, *104* (B2), 2989–3001. <https://doi.org/10.1029/1998jb900047>.
- Godoy, B.; Lazcano, J.; Rodríguez, I.; Martínez, P.; Parada, M. A.; Le Roux, P.; Wilke, H. G.; Polanco, E. Geological Evolution of Paniri Volcano, Central Andes, Northern Chile. *J. South Am. Earth Sci.* **2018**, *84*, 184–200. <https://doi.org/10.1016/j.jsames.2018.03.013>.
- Gogu, R. C.; Dietrich, V. J.; Jenny, B.; Schwandner, F. M.; Hurni, L. A Geo-Spatial Data Management System for Potentially Active Volcanoes - GEOWARN Project. *Comput. Geosci.* **2006**, *32* (1), 29–41. <https://doi.org/10.1016/j.cageo.2005.04.004>.
- Graettinger, A. H.; Ellis, M. K.; Skilling, I. P.; Reath, K.; Ramsey, M. S.; Lee, R. J.; Hughes, C. G.; McGarvie, D. W. Remote Sensing and Geologic Mapping of Glaciovolcanic Deposits in the Region Surrounding Askja (Dyngjufjöll) Volcano, Iceland. *Int. J. Remote Sens.* **2013**, *34* (20), 7178–7198. <https://doi.org/10.1080/01431161.2013.817716>.
- Gray, D. M.; Burton-Johnson, A.; Fretwell, P. T. Evidence for a Lava Lake on Mt. Michael Volcano, Saunders Island (South Sandwich Islands) from Landsat, Sentinel-2 and ASTER Satellite Imagery. *J. Volcanol. Geotherm. Res.* **2019**, *379*, 60–71. <https://doi.org/10.1016/j.jvolgeores.2019.05.002>.
- Grishin, S. Y. Environmental Impact of the Powerful Eruption of Sarychev Peak Volcano (Kuril Islands, 2009) According to Satellite Imagery. *Izv. - Atmos. Ocean Phys.* **2011**, *47* (9), 1028–1031. <https://doi.org/10.1134/S0001433811090064>.
- Grosse, P.; van Wyk de Vries, B.; Euillades, P. A.; Kervyn, M.; Petrinovic, I. A. Systematic Morphometric Characterization of Volcanic Edifices Using Digital Elevation Models. *Geomorphology.* **2012**, *136* (1), 114–131. <https://doi.org/10.1016/j.geomorph.2011.06.001>.
- Gutiérrez, F. J.; Lemus, M.; Parada, M. A.; Benavente, O. M.; Aguilera, F. A. Contribution of Ground Surface Altitude Difference to Thermal Anomaly Detection Using Satellite Images: Application to Volcanic/Geothermal Complexes in the Andes of Central Chile. *J. Volcanol. Geotherm. Res.* **2012**, *237–238*, 69–80. <https://doi.org/10.1016/j.jvolgeores.2012.05.016>.
- Hamlyn, J. E.; Keir, D.; Wright, T. J.; Neuberg, J. W.; Goitom, B.; Hammond, J. O. S.; Pagli, C.; Oppenheimer, C.; Kendall, J. M.; Grandin, R. Seismicity and Subsidence Following the 2011 Nabro Eruption, Eritrea: Insights into the Plumbing System of an off-Rift Volcano. *J. Geophys. Res. Solid Earth.* **2014**, *119* (11), 8267–8282. <https://doi.org/10.1002/2014JB011395>.
- Harris, A. J. L.; Wright, R.; Flynn, L. P. Remote Monitoring of Mount Erebus Volcano, Antarctica, Using Polar Orbiters: Progress and Prospects. *Int. J. Remote Sens.* **1999**, *20* (15–16), 3051–3071. <https://doi.org/10.1080/014311699211615>.
- Harris, A.; Chevrel, M.; Coppola, D.; Ramsey, M.; Hrysiewicz, A.; Thivet, S.; Villeneuve, N.; Favalli, M.; Peltier, A.; Kowalski, P.; et al. Validation of an Integrated Satellite-Data-Driven Response to an Effusive Crisis: The April–May 2018 Eruption of Piton de La Fournaise. *Ann. Geophys.* **2019**, *61* (Vol 61 (2018)), <https://doi.org/10.4401/ag-7972>.
- Head, E. M.; Maclean, A. L.; Carn, S. A. Mapping Lava Flows from Nyamuragira Volcano (1967–2011) with Satellite Data and Automated Classification Methods. *Geomatics, Nat. Hazards Risk.* **2013**, *4* (2), 119–144. <https://doi.org/10.1080/19475705.2012.680503>.
- Hellman, M. J.; Ramsey, M. S. Analysis of Hot Springs and Associated Deposits in Yellowstone National Park Using ASTER and AVIRIS Remote Sensing. *J. Volcanol. Geotherm. Res.* **2004**, *135* (1–2), 195–219. <https://doi.org/10.1016/j.jvolgeores.2003.12.012>.
- Henderson, S. T.; Pritchard, M. E.; Cooper, J. R.; Aoki, Y. Remotely Sensed Deformation and Thermal Anomalies at Mount Pagan, Mariana Islands. *Front. Earth Sci.* **2019**, *7*, 238. <https://doi.org/10.3389/feart.2019.00238>.

- Henney, L. A.; Rodríguez, L. A.; Watson, I. M. A Comparison of SO₂ Retrieval Techniques Using Mini-UV Spectrometers and ASTER Imagery at Lascar Volcano, Chile. *Bull. Volcanol.* **2012**, *74* (2), 589–594. <https://doi.org/10.1007/s00445-011-0552-2>.
- Hirn, B.; Di Bartola, C.; Ferrucci, F. Spaceborne Monitoring 2000–2005 of the Pu’u ’O’o-Kupaianaha (Hawaii) Eruption by Synergetic Merge of Multispectral Payloads ASTER and MODIS. *IEEE Trans. Geosci. Remote Sens.* **2008**, *46* (10), 2848–2856. <https://doi.org/10.1109/TGRS.2008.2001033>.
- Holohan, E. P.; Sudhaus, H.; Walter, T. R.; Schöpfer, M. P. J.; Walsh, J. J. Effects of Host-Rock Fracturing on Elastic-Deformation Source Models of Volcano Deflation. *Sci. Rep.* **2017**, *7* (1), 10970. <https://doi.org/10.1038/s41598-017-10009-6>.
- Hooper, A.; Prata, F.; Sigmundsson, F. Remote Sensing of Volcanic Hazards and Their Precursors. In *Proceedings of the IEEE*; 2012; Vol. 100, pp 2908–2930. <https://doi.org/10.1109/JPROC.2012.2199269>.
- Hubbard, B. E.; Crowley, J. K.; Zimelman, D. R. Comparative Alteration Mineral Mapping Using Visible to Shortwave Infrared (0.4–2.4 Mm) Hyperion, ALI, and ASTER Imagery. *Comp. Gen. Pharmacol.* **2003**, *41* (6), 1401–1410.
- Hubbard, B. E.; Sheridan, M. F.; Carrasco-Núñez, G.; Díaz-Castellón, R.; Rodríguez, S. R. Comparative Lahar Hazard Mapping at Volcan Citlaltépetl, Mexico Using SRTM, ASTER and DTED-1 Digital Topographic Data. *J. Volcanol. Geotherm. Res.* **2007**, *160* (1–2), 99–124. <https://doi.org/10.1016/j.jvolgeores.2006.09.005>.
- Huggel, C.; Caplan-Auerbach, J.; Waythomas, C. F.; Wessels, R. L. Monitoring and Modeling Ice-Rock Avalanches from Ice-Capped Volcanoes: A Case Study of Frequent Large Avalanches on Iliamna Volcano, Alaska. *J. Volcanol. Geotherm. Res.* **2007**, *168* (1–4), 114–136. <https://doi.org/10.1016/j.jvolgeores.2007.08.009>.
- Huggel, C.; Schneider, D.; Miranda, P. J.; Delgado Granados, H.; Käab, A. Evaluation of ASTER and SRTM DEM Data for Lahar Modeling: A Case Study on Lahars from Popocatepetl Volcano, Mexico. *J. Volcanol. Geotherm. Res.* **2008**, *170* (1–2), 99–110. <https://doi.org/10.1016/j.jvolgeores.2007.09.005>.
- Inbar, M.; Gilichinsky, M.; Melekestsev, I.; Melnikov, D.; Zaretskaya, N. Morphometric and Morphological Development of Holocene Cinder Cones: A Field and Remote Sensing Study in the Tolbachik Volcanic Field, Kamchatka. *J. Volcanol. Geotherm. Res.* **2011**, *201* (1–4), 301–311. <https://doi.org/10.1016/j.jvolgeores.2010.07.013>.
- Ino, N.; Toshiaki, Y.; Kinoshita, K. Regional Characteristics of High Concentration Events of Volcanic Gas at Miyakejima. *J. Japan Soc. Nat. Disaster Sci.* **2005**, *23*, 505–520.
- Iwashita, K.; Asaka, T.; Nishikawa, H.; Kondoh, T.; Tahara, T. Vegetation Biomass Change of the Bosoh Peninsula. Impacted by the Volcano Fumes from the Miyakejima. *Adv. Sp. Res.* **2006**, *37* (4), 734–740. <https://doi.org/10.1016/j.asr.2004.12.071>.
- Jay, J. A.; Welch, M.; Pritchard, M. E.; Mares, P. J.; Mnich, M. E.; Melkonian, A. K.; Aguilera, F.; Naranjo, J. A.; Sunagua, M.; Clavero, J. Volcanic Hotspots of the Central and Southern Andes as Seen from Space by ASTER and MODVOLC between the Years 2000 and 2010. *Geol. Soc. Spec. Publ.* **2013**, *380* (1), 161–185. <https://doi.org/10.1144/SP380.1>.
- Jay, J. A.; Delgado, F. J.; Torres, J. L.; Pritchard, M. E.; Macedo, O.; Aguilar, V. Deformation and Seismicity near Sabancaya Volcano, Southern Peru, from 2002 to 2015. *Geophys. Res. Lett.* **2015**, *42* (8), 2780–2788. <https://doi.org/10.1002/2015GL063589>.
- Ji, L. Y.; Xu, J. D.; Lin, X. D.; Luan, P. Application of Satellite Thermal Infrared Remote Sensing in Monitoring Magmatic Activity of Changbaishan Tianchi Volcano. *Chinese Sci. Bull.* **2010**, *55* (24), 2731–2737. <https://doi.org/10.1007/s11434-010-3232-2>.
- Jousset, P.; Pallister, J.; Boichu, M.; Buongiorno, M. F.; Budisantoso, A.; Costa, F.; Andreastuti, S.; Prata, F.; Schneider, D.; et al. The 2010 Explosive Eruption of Java’s Merapi Volcano—A “100-Year” Event. *J. Volcanol. Geotherm. Res.* **2012**, *241–242*, 121–135. <https://doi.org/10.1016/j.jvolgeores.2012.06.018>.

- Joyce, K.; Samsonov, S.; Jolly, G. Satellite Remote Sensing of Volcanic Activity in New Zealand. In Proceedings of the 2008 2nd Workshop on USE of Remote Sensing Techniques for Monitoring Volcanoes and Seismogenic Areas, USEReST; 2008; Vol. 2008, pp 1–4. <https://doi.org/10.1109/USEREST.2008.4740346>.
- Joyce, K. E.; Samsonov, S.; Jolly, G. Temperature, Color and Deformation Monitoring of Volcanic Regions in New Zealand. In *International Geoscience and Remote Sensing Symposium (IGARSS)*; 2009a; Vol. 1; pp 1-17. <https://doi.org/10.1109/IGARSS.2009.5416924>.
- Joyce, K. E.; Samsonov, S.; Manville, V.; Jongens, R.; Graettinger, A.; Cronin, S. J. Remote Sensing Data Types and Techniques for Lahar Path Detection: A Case Study at Mt Ruapehu, New Zealand. *Remote Sens. Environ.* **2009b**, *113* (8), 1778–1786. <https://doi.org/10.1016/j.rse.2009.04.001>.
- Kaneko, T.; Maeno, F.; Yasuda, A. Observation of the Eruption Sequence and Formation Process of a Temporary Lava Lake during the June–August 2015 Mt. Raung Eruption, Indonesia, Using High-Resolution and High-Frequency Satellite Image Datasets. *J. Volcanol. Geotherm. Res.* **2019**, *377*, 17–32. <https://doi.org/10.1016/j.jvolgeores.2019.03.016>.
- Kass, M. A. Slope Stability Analysis of the Iliamna Volcano, Alaska, Using Aster TIR, SRTM Dem, and Aeromagnetic Data. In *Proceedings of the Symposium on the Application of Geophysics to Engineering and Environmental Problems, SAGEEP*; Alaska, 2005; Vol. 2, pp 883–891. <https://doi.org/10.4133/1.2923545>.
- Kearney, C. S.; Dean, K.; Realmuto, V. J.; Watson, I. M.; Dehn, J.; Prata, F. Observations of SO₂ Production and Transport from Bezymianny Volcano, Kamchatka Using the MODerate Resolution Infrared Spectroradiometer (MODIS). *Int. J. Remote Sens.* **2008**, *29* (22), 6647–6665. <https://doi.org/10.1080/01431160802168392>.
- Kereszturi, G.; Procter, J. Error in Topographic Attributes for Volcanic Hazard Assessment of the Auckland Volcanic Field (New Zealand). *New Zeal. J. Geol. Geophys.* **2016**, *59* (2), 286–301. <https://doi.org/10.1080/00288306.2015.1130155>.
- Kern, C.; Masias, P.; Apaza, F.; Reath, K. A.; Platt, U. Remote Measurement of High Preeruptive Water Vapor Emissions at Sabancaya Volcano by Passive Differential Optical Absorption Spectroscopy. *J. Geophys. Res. Solid Earth.* **2017**, *122* (5), 3540–3564. <https://doi.org/10.1002/2017JB014020>.
- Kervyn, M.; Goossens, R.; Jacobs, P.; Ernst, G. G. J. ASTER DEMs for Volcano Topographic Mapping: Accuracy and Limitations. In *IAMG 2006 - 11th International Congress for Mathematical Geology: Quantitative Geology from Multiple Sources*, 2006; pp 1-8.
- Kervyn, M.; Kervyn, F.; Goossens, R.; Rowland, S. K.; Ernst, G. G. J. Mapping Volcanic Terrain Using High-Resolution and 3D Satellite Remote Sensing. *Geol. Soc. Spec. Publ.* **2007**, *283*, 5–30. <https://doi.org/10.1144/SP283.2>.
- Kervyn, M.; Ernst, G. G. J.; Goossens, R.; Jacobs, P. Mapping Volcano Topography with Remote Sensing: ASTER vs. SRTM. *Int. J. Remote Sens.* **2008a**, *29* (22), 6515–6538. <https://doi.org/10.1080/01431160802167949>.
- Kervyn, M.; Ernst, G. G. J.; Harris, A. J. L.; Belton, F.; Mbede, E.; Jacobs, P. Thermal Remote Sensing of the Low-Intensity Carbonatite Volcanism of Oldoinyo Lengai, Tanzania. *Int. J. Remote Sens.* **2008b**, *29* (22), 6467–6499. <https://doi.org/10.1080/01431160802167105>.
- Kervyn, M.; Ernst, G. G. J.; Klaudius, J.; Keller, J.; Mbede, E.; Jacobs, P. Remote Sensing Study of Sector Collapses and Debris Avalanche Deposits at Oldoinyo Lengai and Kerimasi Volcanoes, Tanzania. *Int. J. Remote Sens.* **2008c**, *29* (22), 6565–6595. <https://doi.org/10.1080/01431160802168137>.
- Kim, K.; Lees, J. M. Local Volcano Infrasound and Source Localization Investigated by 3D Simulation. *Seismol. Res. Lett.* **2014**, *85* (6), 1177–1186. <https://doi.org/10.1785/0220140029>.
- Kobayashi, C.; Orihashi, Y.; Hiarata, D.; Naranjo, J. A.; Kobayashi, M.; Anma, R. Compositional Variations Revealed by ASTER Image Analysis of the Viedma Volcano, Southern Andes Volcanic Zone. *Andean Geol.* **2010a**, *37* (2), 433–441.

- Kobayashi, C.; Orihashi, Y.; Hiarata, D.; Naranjo, J. A.; Kobayashi, M.; Anma, R. Spaceborne ASTER Image Analyses Revealed Compositional Variation of the Viedma Volcano in Andean Austral Volcanic Zone. *Andean Geol.* **2010b**, *37* (2), 433–441. <https://doi.org/10.5027/andgeov37n2-a09>.
- Krippner, J. B.; Belousov, A. B.; Belousova, M. G.; Ramsey, M. S. Parametric Analysis of Lava Dome-Collapse Events and Pyroclastic Deposits at Shiveluch Volcano, Kamchatka, Using Visible and Infrared Satellite Data. *J. Volcanol. Geotherm. Res.* **2018**, *354*, 115–129. <https://doi.org/10.1016/j.jvolgeores.2018.01.027>.
- Laiolo, M.; Massimetti, F.; Cigolini, C.; Ripepe, M.; Coppola, D. Long-Term Eruptive Trends from Space-Based Thermal and SO₂ Emissions: A Comparative Analysis of Stromboli, Batu Tara and Tinakula Volcanoes. *Bull. Volcanol.* **2018**, *80* (9), 9. <https://doi.org/10.1007/s00445-018-1242-0>.
- Lara, L. E.; Moreno, R.; Amigo, Á.; Hoblitt, R. P.; Pierson, T. C. Late Holocene History of Chaiten Volcano: New Evidence for a 17th Century Eruption. *Andean Geol.* **2013**, *40* (2), 249–261. <https://doi.org/10.5027/andgeoV40n2-a04>.
- Le Corvec, N.; Spörli, K. B.; Rowland, J.; Lindsay, J. Spatial Distribution and Alignments of Volcanic Centers: Clues to the Formation of Monogenetic Volcanic Fields. *Earth-Science Rev.* **2013**, *124*, 96–114. <https://doi.org/10.1016/j.earscirev.2013.05.005>.
- Mannini, S.; Harris, A. J. L.; Jessop, D. E.; Chevrel, M. O.; Ramsey, M. S. Combining Ground- and ASTER-Based Thermal Measurements to Constrain Fumarole Field Heat Budgets: The Case of Vulcano Fossa 2000–2019. *Geophys. Res. Lett.* **2019**, *46*, 2019. <https://doi.org/10.1029/2019GL084013>.
- Mantas, V. M.; Pereira, A. J. S. C.; Morais, P. V. Plumes of Discolored Water of Volcanic Origin and Possible Implications for Algal Communities. The Case of the Home Reef Eruption of 2006 (Tonga, Southwest Pacific Ocean). *Remote Sens. Environ.* **2011**, *115* (6), 1341–1352. <https://doi.org/10.1016/j.rse.2011.01.014>.
- Mars, J. C. Regional Mapping of Hydrothermally Altered Igneous Rocks along the Urumieh-Dokhtar, Chagai, and Alborz Belts of Western Asia Using Advanced Spaceborne. *US Geol. Surv.* **2014**, *2010-5090-*, 1–46. <https://dx.doi.org/10.3133/sir20105090O>.
- Mars, J. C.; Rowan, L. C. Regional Mapping of Phyllic- and Argillic-Altered Rocks in the Zagros Magmatic Arc, Iran, Using Advanced Spaceborne Thermal Emission and Reflection Radiometer (ASTER) Data and Logical Operator Algorithms. *Geosphere* **2006**, *2* (3), 161–186. <https://doi.org/10.1130/GES00044.1>.
- Mars, J. C.; Rowan, L. C. ASTER Spectral Analysis and Lithologic Mapping of the Khanneshin Carbonatite Volcano, Afghanistan. *Geosphere*. **2011**, *7* (1), 276–289. <https://doi.org/10.1130/GES00630.1>.
- Mars, J. C.; Hubbard, B.; Pieri, D.; Linick, J. Alteration, Slope-Classified Alteration, and Potential Lahar Inundation Maps of Volcanoes for the Advanced Spaceborne Thermal Emission and Reflection Radiometer (ASTER) Volcanoes Archive. *US Geol. Surv.* **2015**, *2015-5035*.
- Mathieu, L.; Kervyn, M.; Ernst, G. G. J. Field Evidence for Flank Instability, Basal Spreading and Volcano-Tectonic Interactions at Mt Cameroon, West Africa. *Bull. Volcanol.* **2011**, *73* (7), 851–867. <https://doi.org/10.1007/s00445-011-0458-z>.
- Mattiou, G. S.; Young, S. R.; Voight, B.; Steven, R.; Sparks, J.; Shalev, E.; Sacks, S.; Malin, P.; Linde, A.; Johnston, W.; et al. Prototype Pbo Instrumentation of Calipso Project Captures World-Record Lava Dome Collapse on Montserrat Volcano. *Eos (Washington, DC)*. **2004**, *85* (34), 317–325. <https://doi.org/10.1029/2004eo340001>.
- McGimsey, R. G.; Neal, C.; Girina, O.; Chibisova, M.; Rybin, A. 2009 Volcanic Activity in Alaska, Kamchatka, and the Kurile Islands — Summary of Events and Response of the Alaska Volcano Observatory Scientific Investigations Report 2013 – 5213. *US Geol. Surv.* **2014**, 1–140.
- Mia, M. B.; Fujimitsu, Y.; Nishijima, J. Exploration and Monitoring of Hatchobaru-Otake Geothermal Field Using ASTER Satellite Images. In *Grand Renewable Energy proceedings Japan council for Renewable Energy*; 2018a; Vol. 276, pp 1–4.

- Mia, M. B.; Fujimitsu, Y.; Nishijima, J. Monitoring Thermal Activity of the Beppu Geothermal Area in Japan Using Multisource Satellite Thermal Infrared Data. *Geosci.* **2018b**, *8* (8), 306. <https://doi.org/10.3390/geosciences8080306>.
- Mia, M. B.; Fujimitsu, Y.; Nishijima, J. Exploration of Hydrothermal Alteration and Monitoring of Thermal Activity Using Multi-Source Satellite Images: A Case Study of the Recently Active Kirishima Volcano Complex on Kyushu Island, Japan. *Geothermics* **2019**, *79*, 26–45. <https://doi.org/10.1016/j.geothermics.2019.01.006>.
- Moran, S. C.; Freymueller, J. T.; LaHusen, R. G.; McGee, K. A.; Poland, M. P.; Power, J. A.; Schmidt, D. A.; Schneider, D. J.; Stephens, G.; Werner, C. A.; White, R.A. *Instrumentation Recommendations for Volcano Monitoring at US Volcanoes under the National Volcano Early Warning System*; 2008; Vol. 5114; pp 1-56.
- Morgado, E.; Morgan, D. J.; Harvey, J.; Parada, M. Á.; Castruccio, A.; Brahm, R.; Gutiérrez, F.; Georgiev, B.; Hammond, S. J. Localised Heating and Intensive Magmatic Conditions Prior to the 22–23 April 2015 Calbuco Volcano Eruption (Southern Chile). *Bull. Volcanol.* **2019**, *81* (4). <https://doi.org/10.1007/s00445-019-1280-2>.
- Moussallam, Y.; Peters, N.; Masias, P.; Apaza, F.; Barnie, T.; Ian Schipper, C.; Curtis, A.; Tamburello, G.; Aiuppa, A.; Bani, P.; et al. Magmatic Gas Percolation through the Old Lava Dome of El Misti Volcano. *Bull. Volcanol.* **2017**, *79* (6), 6. <https://doi.org/10.1007/s00445-017-1129-5>.
- Moyano, J. E. R.; Ulrich, W. K.; Marfull, V. Short Chronological Analysis of the 2007-2009 Eruptive Cycle and Its Nested Cones Formation at Llaima Volcano. *J. Technol. Possibilism.* **2014**, *2* (3), 1–9.
- Muñoz-Salinas, E.; Castillo-Rodríguez, M.; Manea, V.; Manea, M.; Palacios, D. Lahar Flow Simulations Using LAHARZ Program: Application for the Popocatepetl Volcano, Mexico. *J. Volcanol. Geotherm. Res.* **2009**, *182* (1–2), 13–22. <https://doi.org/10.1016/j.jvolgeores.2009.01.030>.
- Murphy, S. W.; De Souza Filho, C. R.; Oppenheimer, C. The Spatial Extent of Thermal Anomalies at Lascar Volcano. *Int. Geosci. Remote Sens. Symp.* **2010**, 1557–1560. <https://doi.org/10.1109/IGARSS.2010.5652858>.
- Murphy, S. W.; Filho, C. R. de S.; Oppenheimer, C. Monitoring Volcanic Thermal Anomalies from Space: Size Matters. *J. Volcanol. Geotherm. Res.* **2011**, *203* (1–2), 48–61. <https://doi.org/10.1016/j.jvolgeores.2011.04.008>.
- Murphy, S. W.; Wright, R.; Oppenheimer, C.; Filho, C. R. S. MODIS and ASTER Synergy for Characterizing Thermal Volcanic Activity. *Remote Sens. Environ.* **2013**, *131*, 195–205. <https://doi.org/10.1016/j.rse.2012.12.005>.
- Nakada, S.; Zaennudin, A.; Yoshimoto, M.; Maeno, F.; Suzuki, Y.; Hokanishi, N.; Sasaki, H.; Iguchi, M.; Ohkura, T.; Gunawan, H.; et al. Growth Process of the Lava Dome/Flow Complex at Sinabung Volcano during 2013–2016. *J. Volcanol. Geotherm. Res.* **2019**, *382*, 120–136. <https://doi.org/10.1016/j.jvolgeores.2017.06.012>.
- Naranjo, M. F.; Ebmeier, S. K.; Vallejo, S.; Ramón, P.; Mothes, P.; Biggs, J.; Herrera, F. Mapping and Measuring Lava Volumes from 2002 to 2009 at El Reventador Volcano, Ecuador, from Field Measurements and Satellite Remote Sensing. *J. Appl. Volcanol.* **2016**, *5* (1), 1. <https://doi.org/10.1186/s13617-016-0048-z>.
- Oikonomidis, D.; Albanakis, K.; Pavlides, S.; Fytikas, M. Reconstruction of the Paleo-Coastline of Santorini Island (Greece), after the 1613 BC Volcanic Eruption: A GIS-Based Quantitative Methodology. *J. Earth Syst. Sci.* **2016**, *125* (1), 1–11. <https://doi.org/10.1007/s12040-015-0643-0>.
- Oppenheimer, C. Crater Lake Heat Losses Estimated by Remote Sensing. *Geophys. Res. Lett.* **1996**, *23* (14), 1793–1796. <https://doi.org/10.1029/96GL01591>.
- Oppenheimer, C. Remote Sensing of the Colour and Temperature of Volcanic Lakes. *Int. J. Remote Sens.* **1997**, *18* (1), 5–37. <https://doi.org/10.1080/014311697219259>.
- Oppenheimer, C.; Francis, P.; Burton, M.; Maciejewski, A. J. H.; Boardman, L. Remote Measurement of Volcanic Gases by Fourier Transform Infrared Spectroscopy. *Appl. Phys. B Lasers Opt.* **1998**, *67* (4), 505–515. <https://doi.org/10.1007/s003400050536>.

- Paguican, E. M. R.; Lagmay, A. M. F.; Rodolfo, K. S.; Rodolfo, R. S.; Tengonciang, A. M. P.; Lapus, M. R.; Baliatan, E. G.; Obille, E. C. Extreme Rainfall-Induced Lahars and Dike Breaching, 30 November 2006, Mayon Volcano, Philippines. *Bull. Volcanol.* **2009**, *71* (8), 845–857. <https://doi.org/10.1007/s00445-009-0268-8>.
- Pallister, J.; Wessels, R.; Griswold, J.; McCausland, W.; Kartadinata, N.; Gunawan, H.; Budianto, A.; Primulyana, S. Monitoring, Forecasting Collapse Events, and Mapping Pyroclastic Deposits at Sinabung Volcano with Satellite Imagery. *J. Volcanol. Geotherm. Res.* **2019**, *382*, 149–163. <https://doi.org/10.1016/j.jvolgeores.2018.05.012>.
- Patrick, M. R.; Witzke, C.-N. Thermal Mapping of Hawaiian Volcanoes with ASTER Satellite Data. *U.S. Geol. Surv. Sci. Investig. Rep. 2011–5110* **2011**, 22 p.
- Patrick, M. R.; Orr, T. R. Rootless Shield and Perched Lava Pond Collapses at Kilauea Volcano, Hawai'i. *Bull. Volcanol.* **2012**, *74* (1), 67–78. <https://doi.org/10.1007/s00445-011-0505-9>.
- Patrick, M.; Dean, K.; Dehn, J. Active Mud Volcanism Observed with Landsat 7 ETM+. *J. Volcanol. Geotherm. Res.* **2004**, *131* (3–4), 307–320. [https://doi.org/10.1016/S0377-0273\(03\)00383-4](https://doi.org/10.1016/S0377-0273(03)00383-4).
- Patrick, M. R.; Smellie, J. L.; Harris, A. J. L.; Wright, R.; Dean, K.; Izbekov, P.; Garbeil, H.; Pilger, E. First Recorded Eruption of Mount Belinda Volcano (Montagu Island), South Sandwich Islands. *Bull. Volcanol.* **2005**, *67* (5), 415–422. <https://doi.org/10.1007/s00445-004-0382-6>.
- Patrick, M. R.; Kauahikaua, J.; Orr, T.; Davies, A.; Ramsey, M. Operational Thermal Remote Sensing and Lava Flow Monitoring at the Hawaiian Volcano Observatory. *Geol. Soc. Spec. Publ.* **2016**, *426* (1), 489–503. <https://doi.org/10.1144/SP426.17>.
- Pavez, A.; Remy, D.; Bonvalot, S.; Diament, M.; Gabalda, G.; Froger, J. L.; Julien, P.; Legrand, D.; Moisset, D. Insight into Ground Deformations at Lascar Volcano (Chile) from SAR Interferometry, Photogrammetry and GPS Data: Implications on Volcano Dynamics and Future Space Monitoring. *Remote Sens. Environ.* **2006**, *100* (3), 307–320. <https://doi.org/10.1016/j.rse.2005.10.013>.
- Permenter, J. L.; Oppenheimer, C. Volcanoes of the Tibesti Massif (Chad, Northern Africa). *Bull. Volcanol.* **2007**, *69* (6), 609–626. <https://doi.org/10.1007/s00445-006-0098-x>.
- Pieri, D.; Abrams, M. ASTER Watches the World's Volcanoes: A New Paradigm for Volcanological Observations from Orbit. *J. Volcanol. Geotherm. Res.* **2004**, *135* (1–2), 13–28. <https://doi.org/10.1016/j.jvolgeores.2003.12.018>.
- Pieri, D.; Abrams, M. ASTER Observations of Thermal Anomalies Preceding the April 2003 Eruption of Chikurachki Volcano, Kurile Islands, Russia. *Remote Sens. Environ.* **2005**, *99* (1–2), 84–94. <https://doi.org/10.1016/j.rse.2005.06.012>.
- Pieri, D. C.; Crisp, J.; Kahle, A. B. Observing Volcanism and Other Transient Phenomena with ASTER. *J. Remote Sens. Soc. Japan.* **1995**, *15* (2), 148–153. <https://doi.org/10.1144/rssj1981.15.148>.
- Pieri, D.; Diaz, J. A.; Bland, G.; Fladeland, M.; Madrigal, Y.; Corrales, E.; Alegria, O.; Alan, A.; Realmuto, V.; Miles, T.; et al. In Situ Observations and Sampling of Volcanic Emissions with NASA and UCR Unmanned Aircraft, Including a Case Study at Turrialba Volcano, Costa Rica. *Geol. Soc. Spec. Publ.* **2013**, *380* (1), 321–352. <https://doi.org/10.1144/SP380.13>.
- Pinardi, G.; Campion, R.; Roozendaal, M. Van; Fayt, C.; Geffen, J. Van; Galle, B. Comparison of Volcanic SO₂ Flux Measurements from Satellite and from the NOVAC Network. In *EUMETSAT conference*; 2010; Vol. 2, pp1-8.
- Piscini, A.; Amici, S.; Fieri, D. Spectral Analysis of ASTER and Hyperion Data for Geological Classification of Volcano Teide. *International Geoscience and Remote Sensing Symposium (IGARSS)*. 2010, pp 2267–2270. <https://doi.org/10.1109/IGARSS.2010.5652063>.
- Plank, S.; Nolde, M.; Richter, R.; Fischer, C.; Martinis, S.; Riedlinger, T.; Schoepfer, E.; Klein, D. Monitoring of the 2015 Villarrica Volcano Eruption by Means of DLR's Experimental TET-1 Satellite. *Remote Sens.* **2018**, *10* (9), 9. <https://doi.org/10.3390/rs10091379>.

- Prambada, O.; Arakawa, Y.; Ikehata, K.; Furukawa, R.; Takada, A.; Wibowo, H. E.; Nakagawa, M.; Kartadinata, M. N. Eruptive History of Sundoro Volcano, Central Java, Indonesia since 34 Ka. *Bull. Volcanol.* **2016**, *78* (11), 11. <https://doi.org/10.1007/s00445-016-1079-3>.
- Price, M. A.; Ramsey, M. S.; Crown, D. A. Satellite-Based Thermophysical Analysis of Volcaniclastic Deposits: A Terrestrial Analog for Mantled Lava Flows on Mars. *Remote Sens.* **2016**, *8* (2), 152. <https://doi.org/10.3390/rs8020152>.
- Pritchard, M. E.; Jay, J. A.; Aron, F.; Henderson, S. T.; Lara, L. E. Subsidence at Southern Andes Volcanoes Induced by the 2010 Maule, Chile Earthquake. *Nat. Geosci.* **2013**, *6* (8), 632–636. <https://doi.org/10.1038/ngeo1855>.
- Pritchard, M. E.; Henderson, S. T.; Jay, J. A.; Soler, V.; Krzesni, D. A.; Button, N. E.; Welch, M. D.; Semple, A. G.; Glass, B.; Sunagua, M.; et al. Reconnaissance Earthquake Studies at Nine Volcanic Areas of the Central Andes with Coincident Satellite Thermal and InSAR Observations. *J. Volcanol. Geotherm. Res.* **2014**, *280*, 90–103. <https://doi.org/10.1016/j.jvolgeores.2014.05.004>.
- Pugnaghi, S.; Gangale, G.; Corradini, S.; Buongiorno, M. F. Mt. Etna Sulfur Dioxide Flux Monitoring Using ASTER-TIR Data and Atmospheric Observations. *J. Volcanol. Geotherm. Res.* **2006**, *152* (1–2), 74–90.
- Raharimahefa, T.; Rasoazanamparany, C. Geomorphological Classification of Volcanic Cones in the Itasy Volcanic Field, Central Madagascar. *Int. J. Geol. Earth Sci.* **2018**, *4* (4), 14. <https://doi.org/10.32937/ijges.4.4.2018.14-34>.
- Ramsey, M. S. Temperature and Textures of Ash Flow Surfaces: Sheveluch, Kamchatka, Russia (2004). In *Monitoring Volcanoes in the North Pacific*; Dean, K. G., Dehn, J., Eds.; **2015**; pp 79–100. <https://doi.org/10.1007/978-3-540-68750-4>.
- Ramsey, M. S. Synergistic Use of Satellite Thermal Detection and Science: A Decadal Perspective Using ASTER. *Geol. Soc. Spec. Publ.* **2016**, *426* (1), 115–136. <https://doi.org/10.1144/SP426.23>.
- Ramsey, M. S.; Fink, J. H. Estimating Silicic Lava Vesicularity with Thermal Remote Sensing: A New Technique for Volcanic Mapping and Monitoring. *Bull. Volcanol.* **1999**, *61* (1–2), 32–39. <https://doi.org/10.1007/s004450050260>.
- Ramsey, M. S.; Flynn, L. P. Strategies, Insights, and the Recent Advances in Volcanic Monitoring and Mapping with Data from NASA's Earth Observing System. *J. Volcanol. Geotherm. Res.* **2004**, *135* (1–2), 1–11. <https://doi.org/10.1016/j.jvolgeores.2003.12.015>.
- Ramsey, M.; Dehn, J. Spaceborne Observations of the 2000 Bezymianny, Kamchatka Eruption: The Integration of High-Resolution ASTER Data into near Real-Time Monitoring Using AVHRR. *J. Volcanol. Geotherm. Res.* **2004**, *135* (1–2), 127–146. <https://doi.org/10.1016/j.jvolgeores.2003.12.014>.
- Ramsey, M. S.; Harris, A. J. L. Volcanology 2020: How Will Thermal Remote Sensing of Volcanic Surface Activity Evolve over the next Decade? *J. Volcanol. Geotherm. Res.* **2013**, *249*, 217–233. <https://doi.org/10.1016/j.jvolgeores.2012.05.011>.
- Ramsey, M. S.; Wessels, R. L.; Anderson, S. W. Surface Textures and Dynamics of the 2005 Lava Dome at Shiveluch Volcano, Kamchatka. *Bull. Geol. Soc. Am.* **2012**, *124* (5–6), 678–689. <https://doi.org/10.1130/B30580.1>.
- Ramsey, M. S.; Harris, A. J. L.; Crown, D. A. What Can Thermal Infrared Remote Sensing of Terrestrial Volcanoes Tell Us about Processes Past and Present on Mars? *J. Volcanol. Geotherm. Res.* **2016**, *311*, 198–216. <https://doi.org/10.1016/j.jvolgeores.2016.01.012>.
- Ramsey, M. S.; Chevrel, M. O.; Coppola, D.; Harris, A. J. L. The Influence of Emissivity on the Thermo-Rheological Modeling of the Channelized Lava Flows at Tolbachik Volcano. *Ann. Geophys.* **2019**, *62* (Special Issue), 2. <https://doi.org/10.4401/ag-8077>.
- Rathnam, S. M.; Ramashri, T. Identification of Volcano Hotspots in Multi Spectral ASTER Satellite Images Using DTCWT Image Fusion and ANFIS Classifier. *Am. J. Eng. Res. (AJER)*, **2016a**, *12* (12), 21–31.

- Rathnam, S. M.; Ramashri, T. Identification of Volcano Hotspots Using Multispectral ASTER Satellite Images. *Int. J. Comput. Sci. Inf. Secur.* **2016b**, *14* (10), 138.
- Realmuto, V. J.; Sutton, A. J.; Elias, T. Multispectral Thermal Infrared Mapping of Sulfur Dioxide Plumes: A Case Study from the East Rift Zone of Kilauea Volcano, Hawaii. *J. Geophys. Res. Solid Earth.* **1997**, *102* (B7), 15057–15072. <https://doi.org/10.1029/96jb03916>.
- Realmuto, V. J. The potential use of the earth observing system data to monitor the passive emissions of sulfur dioxide from volcanoes. *Geophys. Monogr. Ser.* **2000**, *116*, 101–115. <https://doi.org/10.1029/GM116pp0101>.
- Realmuto, V. J.; Worden, H. M. Impact of Atmospheric Water Vapor on the Thermal Infrared Remote Sensing of Volcanic Sulfur Dioxide Emissions: A Case Study from the Pu'u 'O' Vent of Kilauea Volcano, Hawaii. *J. Geophys. Res. Solid Earth.* **2000**, *105* (B9), 21497–21507. <https://doi.org/10.1029/2000jb900172>.
- Realmuto, V. J.; Berk, A. Plume Tracker: Interactive Mapping of Volcanic Sulfur Dioxide Emissions with High-Performance Radiative Transfer Modeling. *J. Volcanol. Geotherm. Res.* **2016**, *327*, 55–69. <https://doi.org/10.1016/j.jvolgeores.2016.07.001>.
- Reath, K.; Ramsey, M. S.; Dehn, J.; Webley, P. W. Predicting Eruptions from Precursory Activity Using Remote Sensing Data Hybridization. *J. Volcanol. Geotherm. Res.* **2016**, *321*, 18–30. <https://doi.org/10.1016/j.jvolgeores.2016.04.027>.
- Reath, K.; Pritchard, M. E.; Moruzzi, S.; Alcott, A.; Coppola, D.; Pieri, D. The AVTOD (ASTER Volcanic Thermal Output Database) Latin America Archive. *J. Volcanol. Geotherm. Res.* **2019**, *376*, 62–74. <https://doi.org/10.1016/j.jvolgeores.2019.03.019>.
- Rivera, M.; Thouret, J. C.; Samaniego, P.; Le Pennec, J. L. The 2006–2009 Activity of the Ubinas Volcano (Peru): Petrology of the 2006 Eruptive Products and Insights into Genesis of Andesite Magmas, Magma Recharge and Plumbing System. *J. Volcanol. Geotherm. Res.* **2014**, *270*, 122–141. <https://doi.org/10.1016/j.jvolgeores.2013.11.010>.
- Robertson, E.; Biggs, J.; Edmonds, M.; Clor, L.; Fischer, T. P.; Vye-Brown, C.; Kianji, G.; Koros, W.; Kandie, R. Diffuse Degassing at Longonot Volcano, Kenya: Implications for CO₂ Flux in Continental Rifts. *J. Volcanol. Geotherm. Res.* **2016**, *327*, 208–222. <https://doi.org/10.1016/j.jvolgeores.2016.06.016>.
- Rogic, N.; Cappello, A.; Ferrucci, F. Role of Emissivity in Lava Flow 'Distance-to-Run' Estimates from Satellite-Based Volcano Monitoring. *Remote Sens.* **2019**, *11* (6), 662. <https://doi.org/10.3390/rs11060662>.
- Rose, S.; Ramsey, M. S. The 2005 Eruption of Kliuchevskoi Volcano: Chronology and Processes Derived from ASTER Spaceborne and Field-Based Data. *J. Volcanol. Geotherm. Res.* **2009**, *184* (3–4), 367–380. <https://doi.org/10.1016/j.jvolgeores.2009.05.001>.
- Rose, S. R.; Ramsey, M. S. The 2005 and 2007 Eruptions of Klyuchevskoy Volcano, Russia: Behavior and Effusion Mechanisms. In *Monitoring Volcanoes in the North Pacific: Observations from Space*; Dean, K. G., Dehn, J., Eds.; - 540-24125-6, 389 pp: DVD), Springer-Praxis Books, ISBN, **2015**; pp 973–978.
- Rose, S. R.; Watson, I. M.; Ramsey, M. S.; Hughes, C. G. Thermal Deconvolution: Accurate Retrieval of Multispectral Infrared Emissivity from Thermally-Mixed Volcanic Surfaces. *Remote Sens. Environ.* **2014**, *140*, 690–703. <https://doi.org/10.1016/j.rse.2013.10.009>.
- Roverato, M.; Capra, L.; Sulpizio, R. First Evidence of Hydromagmatism at Colima Volcano (Mexico). *J. Volcanol. Geotherm. Res.* **2013**, *249*, 197–200. <https://doi.org/10.1016/j.jvolgeores.2012.10.012>.
- Rowan, L. C.; Hook, S. J.; Abrams, M. J.; Mars, J. C. Mapping Hydrothermally Altered Rocks at Cuprite, Nevada, Using the Advanced Spaceborne Thermal Emission and Reflection Radiometer (ASTER), a New Satellite-Imaging System. *Econ. Geol.* **2003**, *98* (5), 1019–1027. <https://doi.org/10.2113/gsecongeo.98.5.1019>.
- Rowan, L. C.; Schmidt, R. G.; Mars, J. C. Distribution of Hydrothermally Altered Rocks in the Reko Diq, Pakistan Mineralized Area Based on Spectral Analysis of ASTER Data. *Remote Sens. Environ.* **2006**, *104* (1), 74–87. <https://doi.org/https://doi.org/10.1016/j.rse.2006.05.014>.

- Rybin, A.; Chibisova, M.; Webley, P.; Steensen, T.; Izbekov, P.; Neal, C.; Realmuto, V. Satellite and Ground Observations of the June 2009 Eruption of Sarychev Peak Volcano, Matua Island, Central Kuriles. *Bull. Volcanol.* **2011**, *73* (9), 1377–1392. <https://doi.org/10.1007/s00445-011-0481-0>.
- Saepuloh, A.; Koike, K.; Sumintadireja, P.; Nugraha, A. Digital Geological Mapping Using ASTER Level-1B in Relation with Heat Source of Geothermal System in an Active Volcano. *ISTECS* **2008**, *X*, 1–11.
- Saepuloh, A.; Urai, M.; Widiwijayanti, C.; Aisyah, N. Observing 2006–2010 Ground Deformations of Merapi Volcano (Indonesia) Using ALOS/PALSAR and ASTER TIR Data. In *International Geoscience and Remote Sensing Symposium (IGARSS)*; 2011; pp 1634–1637. <https://doi.org/10.1109/IGARSS.2011.6049545>.
- Saepuloh, A.; Urai, M.; Aisyah, N.; Sunarta; Widiwijayanti, C.; Subandriyo; Jousset, P. Interpretation of Ground Surface Changes Prior to the 2010 Large Eruption of Merapi Volcano Using ALOS/PALSAR, ASTER TIR and Gas Emission Data. *J. Volcanol. Geotherm. Res.* **2013**, *261*, 130–143. <https://doi.org/10.1016/j.jvolgeores.2013.05.001>.
- Sasai, Y.; Hapada, M.; Sabit, J. P.; Zlotnickl, J.; Tanaka, Y.; Cordon Jr., J. M.; Uyeda, S.; Nagao, T.; Sincioco, J. S. Geomagnetic and Topographic Survey of the Main Crater Lake in Taal Volcano (Philippines): Preliminary Report. *Chigaku Zasshi (Journal Geogr.* **2008**, *117* (5), 894–900. <https://doi.org/10.5026/jgeography.117.894>.
- Schneider, D.; Delgado Granados, H.; Huggel, C.; Käab, A. Assessing Lahars from Ice-Capped Volcanoes Using ASTER Satellite Data, the SRTM DTM and Two Different Flow Models: Case Study on Iztaccihuatl (Central Mexico). *Nat. Hazards Earth Syst. Sci.* **2008**, *8* (3), 559–571. <https://doi.org/10.5194/nhess-8-559-2008>.
- Scholte, K. H.; Hommels, A.; Meer, F. D.; Kroonenberg, S. B.; Hanssen, R. G.; Aliyeva, E. Preliminary Aster and InSAR Imagery Combination for Mud Volcano Dynamics, Azerbaijan. In *International Geoscience and Remote Sensing Symposium*; 2003; Vol. 3, pp 13–16.
- Sekertekin, A.; Arslan, N. Monitoring Thermal Anomaly and Radiative Heat Flux Using Thermal Infrared Satellite Imagery – A Case Study at Tuzla Geothermal Region. *Geothermics.* **2019**, *78*, 243–254. <https://doi.org/10.1016/j.geothermics.2018.12.014>.
- Selles, A.; Deffontaines, B.; Hendrayana, H.; Violette, S. The Eastern Flank of the Merapi Volcano (Central Java, Indonesia): Architecture and Implications of Volcaniclastic Deposits. *J. Asian Earth Sci.* **2015**, *108*, 33–47. <https://doi.org/10.1016/j.jseaes.2015.04.026>.
- Silvestri, M.; Cardellini, C.; Chiodini, G.; Buongiorno, M. F. Satellite-Derived Surface Temperature and in Situ Measurement at Solfatara of Pozzuoli (Naples, Italy). *Geochemistry, Geophys. Geosystems.* **2016**, *17* (6), 2095–2109. <https://doi.org/10.1002/2015GC006195>.
- Silvestri, M.; Rabuffi, F.; Pisciotta, A.; Musacchio, M.; Diliberto, I. S.; Spinetti, C.; Lombardo, V.; Colini, L.; Buongiorno, M. F. Analysis of Thermal Anomalies in Volcanic Areas Using Multiscale and Multitemporal Monitoring: Vulcano Island Test Case. *Remote Sens.* **2019**, *11* (2), 2. <https://doi.org/10.3390/rs11020134>.
- Smets, B.; D'Oreye, N.; Kervyn, F.; Kervyn, M.; Albino, F.; Arellano, S. R.; Bagalwa, M.; Balagizi, C.; Carn, S. A.; Darrah, T. H.; et al. Detailed Multidisciplinary Monitoring Reveals Pre- and Co-Eruptive Signals at Nyamulagira Volcano (North Kivu, Democratic Republic of Congo). *Bull. Volcanol.* **2014**, *76* (1), 1–35. <https://doi.org/10.1007/s00445-013-0787-1>.
- Solikhin, A.; Thouret, J. C.; Gupta, A.; Harris, A. J. L.; Liew, S. C. Geology, Tectonics, and the 2002–2003 Eruption of the Semeru Volcano, Indonesia: Interpreted from High-Spatial Resolution Satellite Imagery. *Geomorphology* **2012**, *138* (1), 364–379. <https://doi.org/10.1016/j.geomorph.2011.10.001>.
- Sosio, R.; Crosta, G. B.; Hungr, O. Numerical Modeling of Debris Avalanche Propagation from Collapse of Volcanic Edifices. *Landslides* **2012**, *9* (3), 315–334. <https://doi.org/10.1007/s10346-011-0302-8>.
- Spinetti, C.; Buongiorno, M. F.; Silvestri, M.; Zoffoli, S. Mt. Etna Volcanic Plume from ASTER and HYPERION Data by ASI-SRV Modules. *Int. Geosci. Remote Sens. Symp.* **2011**, No. July, 4018–4021. <https://doi.org/10.1109/IGARSS.2011.6050113>.

- Spinetti, C.; Barsotti, S.; Neri, A.; Buongiorno, M. F.; Doumaz, F.; Nannipieri, L. Investigation of the Complex Dynamics and Structure of the 2010 Eyjafjallajökull Volcanic Ash Cloud Using Multispectral Images and Numerical Simulations. *J. Geophys. Res. Atmos.* **2013**, *118* (10), 4729–4747. <https://doi.org/10.1002/jgrd.50328>.
- Stebel, K.; Amigo, A.; Thomas, H.; Prata, A. J. First Estimates of Fumarolic SO₂ Fluxes from Putana Volcano, Chile, Using an Ultraviolet Imaging Camera. *J. Volcanol. Geotherm. Res.* **2015**, *300*, 112–120. <https://doi.org/10.1016/j.jvolgeores.2014.12.021>.
- Stevens, N. F.; Garbeil, H.; Mouginiis-Mark, P. J. NASA EOS Terra ASTER: Volcanic Topographic Mapping and Capability. *Remote Sens. Environ.* **2004**, *90* (3), 405–414. <https://doi.org/10.1016/j.rse.2004.01.012>.
- Suminar, W.; Saepuloh, A.; Meilano, I. Identifying Hazard Parameter to Develop Quantitative and Dynamic Hazard Map of an Active Volcano in Indonesia. *AIP Conf. Proc.* **2016**, *1730*, 1. <https://doi.org/10.1063/1.4947403>.
- Takarada, S. The Volcanic Hazards Assessment Support System for the Online Hazard Assessment and Risk Mitigation of Quaternary Volcanoes in the World. *Front. Earth Sci.* **2017**, *5*, 14. <https://doi.org/10.3389/feart.2017.00102>.
- Tayebi, M. H.; Tangestani, M. H.; Vincent, R. K.; Neal, D. Spectral Properties and ASTER-Based Alteration Mapping of Masahim Volcano Facies, SE Iran. *J. Volcanol. Geotherm. Res.* **2014**, *287*, 40–50. <https://doi.org/10.1016/j.jvolgeores.2014.09.013>.
- Thomas, H. E.; Watson, I. M. Observations of Volcanic Emissions from Space: Current and Future Perspectives. *Nat. Hazards* **2010**, *54* (2), 323–354. <https://doi.org/10.1007/s11069-009-9471-3>.
- Thompson, J. O.; Ramsey, M. S.; Hall, J. L. MMT-Cam: A New Miniature Multispectral Thermal Infrared Camera System for Capturing Dynamic Earth Processes. *IEEE Trans. Geosci. Remote Sens.* **2019**, *57* (10), 7438–7446. <https://doi.org/10.1109/tgrs.2019.2913344>.
- Torres, R.; Mouginiis-Mark, P.; Self, S.; Garbeil, H.; Kallianpur, K.; Quiambao, R. Monitoring the Evolution of the Pasig-Potrero Alluvial Fan, Pinatubo Volcano, Using a Decade of Remote Sensing Data. *J. Volcanol. Geotherm. Res.* **2004**, *138* (3–4), 371–392. <https://doi.org/10.1016/j.jvolgeores.2004.08.005>.
- Tralli, D. M.; Blom, R. G.; Zlotnicki, V.; Donnellan, A.; Evans, D. L. Satellite Remote Sensing of Earthquake, Volcano, Flood, Landslide and Coastal Inundation Hazards. *ISPRS J. Photogramm. Remote Sens.* **2005**, *59* (4), 185–198. <https://doi.org/10.1016/j.isprsjprs.2005.02.002>.
- Troncoso, L.; Bustillos, J.; Romero, J. E.; Guevara, A.; Carrillo, J.; Montalvo, E.; Izquierdo, T. Hydrovolcanic Ash Emission between August 14 and 24, 2015 at Cotopaxi Volcano (Ecuador): Characterization and Eruption Mechanisms. *J. Volcanol. Geotherm. Res.* **2017**, *341*, 228–241. <https://doi.org/10.1016/j.jvolgeores.2017.05.032>.
- Trunk, L.; Bernard, A. Investigating Crater Lake Warming Using ASTER Thermal Imagery: Case Studies at Ruapehu, Poás, Kawah Ijen, and Copahué Volcanoes. *J. Volcanol. Geotherm. Res.* **2008**, *178* (2), 259–270. <https://doi.org/10.1016/j.jvolgeores.2008.06.020>.
- Tsu, H.; Yamaguchi, Y.; Fujisada, H.; Kahle, A.; Sato, I.; Kato, M.; Watanabe, H.; Kudoh, M.; Pniel, M. ASTER Early Science Outcome and Operation Status. *Sensors, Syst. Next-Generation Satell.* **2001**, *4169* (IV), 1–8.
- Ulusoy, İ. Temporal Radiative Heat Flux Estimation and Alteration Mapping of Tendürek Volcano (Eastern Turkey) Using ASTER Imagery. *J. Volcanol. Geotherm. Res.* **2016**, *327*, 40–54. <https://doi.org/10.1016/j.jvolgeores.2016.06.027>.
- Urai, M. Observation of SO₂ in Miyakejima Island by ASTER, MODIS; *Occasional Papers. Research Center for the Pacific Island, Kagoshima University* 2003; Vol. 37, 50–57.
- Urai, M. Sulfur Dioxide Flux Estimation from Volcanoes Using Advanced Spaceborne Thermal Emission and Reflection Radiometer - a Case Study of Miyakejima Volcano, Japan. *J. Volcanol. Geotherm. Res.* **2004**, *134* (1–2), 1–13. <https://doi.org/10.1016/j.jvolgeores.2003.11.008>.

- Urai, M. Volcano Observations with ASTER and ASTER Image Database for Volcanoes. In *International Geoscience and Remote Sensing Symposium (IGARSS)*; 2011; pp 3661–3663. <https://doi.org/10.1109/IGARSS.2011.6050018>.
- Urai, M.; Pieri, D. ASTER Applications in Volcanology. In *Remote Sensing and Digital Image Processing*; Ramachandran, B., Justice, C., Abrams, M., Eds.; NASA's Earth Observing System and the Science of ASTER and MODIS. Springer, New York, Land Remote Sensing and Global Environmental Change, 2011; Vol. 11, pp 245–272. https://doi.org/10.1007/978-1-4419-6749-7_12.
- Urai, M.; Fukui, K.; Yamaguchi, Y.; Pieri, D. Volcano Observation Potential and Global Volcano Monitoring Plan with ASTER. *Bull. Volcanol. Soc. Japan*. **1999**, *44* (3), 131–141. https://doi.org/10.18940/kazan.44.3_131.
- Urai, M.; Kawanabe, Y.; Itoh, J.; Takada, A.; Kato, M. Ash Fall Areas Associated with the Usu 2000 Eruption Observed by ASTER. *Bull. Geol. Surv. Japan*. **2001**, *52* (4–5), 189–197. <https://doi.org/10.9795/bullgsj.52.189>.
- Urai, M.; Geshi, N.; Staudacher, T. Size and Volume Evaluation of the Caldera Collapse on Piton de La Fournaise Volcano during the April 2007 Eruption Using ASTER Stereo Imagery. *Geophys. Res. Lett.* **2007**, *34* (22), L22318–L22318. <https://doi.org/10.1029/2007GL031551>.
- Urai, M.; Ishizuka, Y. Advantages and Challenges of Space-Borne Remote Sensing for Volcanic Explosivity Index (VEI): The 2009 Eruption of Sarychev Peak on Matua Island, Kuril Islands, Russia. *J. Volcanol. Geotherm. Res.* **2011**, *208* (3–4), 163–168. <https://doi.org/10.1016/j.jvolgeores.2011.07.010>.
- Vaughan, R. G.; Hook, S. J. Using Satellite Data to Characterize the Temporal Thermal Behavior of an Active Volcano: Mount St. Helens, WA. *Geophys. Res. Lett.* **2006**, *33* (20), L20303–L20303. <https://doi.org/10.1029/2006GL027957>.
- Vaughan, R. G.; Abrams, M. J.; Hook, S. J.; Pieri, D. C. Satellite Observations of New Volcanic Island in Tonga. *Eos (Washington, DC)*. **2007**, *88* (4), 37–41. <https://doi.org/10.1029/2007EO040002>.
- Vaughan, R. G.; Kervyn, M.; Realmuto, V.; Abrams, M.; Hook, S. J. Satellite Measurements of Recent Volcanic Activity at Oldoinyo Lengai, Tanzania. *J. Volcanol. Geotherm. Res.* **2008**, *173* (3–4), 196–206. <https://doi.org/10.1016/j.jvolgeores.2008.01.028>.
- Vaughan, R. G.; Keszthelyi, L. P.; Davies, A. G.; Schneider, D. J.; Jaworowski, C.; Heasler, H. Exploring the Limits of Identifying Sub-Pixel Thermal Features Using ASTER TIR Data. *J. Volcanol. Geotherm. Res.* **2010**, *189* (3–4), 225–237. <https://doi.org/10.1016/j.jvolgeores.2009.11.010>.
- Vaughan, R. G.; Keszthelyi, L. P.; Lowenstern, J. B.; Jaworowski, C.; Heasler, H. Use of ASTER and MODIS Thermal Infrared Data to Quantify Heat Flow and Hydrothermal Change at Yellowstone National Park. *J. Volcanol. Geotherm. Res.* **2012a**, *233–234*, 72–89. <https://doi.org/10.1016/j.jvolgeores.2012.04.022>.
- Vaughan, R. G.; Lowenstern, J. B.; Keszthelyi, L. P.; Jaworowski, C.; Heasler, H. Mapping Temperature and Radiant Geothermal Heat Flux Anomalies in the Yellowstone Geothermal System Using ASTER Thermal Infrared Data. *Trans. - Geotherm. Resour. Counc.* **2012b**, *36* (2), 1403–1409.
- Viramonte, J.; Godoy, S.; Arnosio, M.; Becchio, R.; Poodts, M. El Campo Geotermal de La Caldera Del Cerro Blanco: Utilización de Imágenes Aster. *Buenos Aires, Asoc. Geológica Argentina* **2005**, *2*, 505–512.
- Völker, D.; Kutterolf, S.; Wehrmann, H. Comparative Mass Balance of Volcanic Edifices at the Southern Volcanic Zone of the Andes between 33°S and 46°S. *J. Volcanol. Geotherm. Res.* **2011**, *205* (3–4), 114–129. <https://doi.org/10.1016/j.jvolgeores.2011.03.011>.
- Volynets, A. O.; Edwards, B. R.; Melnikov, D.; Yakushev, A.; Griboedova, I. Monitoring of the Volcanic Rock Compositions during the 2012–2013 Fissure Eruption at Tolbachik Volcano, Kamchatka. *J. Volcanol. Geotherm. Res.* **2015**, *307*, 120–132. <https://doi.org/10.1016/j.jvolgeores.2015.07.014>.
- Wadge, G.; Burt, L. Stress Field Control of Eruption Dynamics at a Rift Volcano: Nyamuragira, D.R.Congo. *J. Volcanol. Geotherm. Res.* **2011**, *207* (1–2), 1–15. <https://doi.org/10.1016/j.jvolgeores.2011.06.012>.

- Wadge, G.; Saunders, S.; Itikarai, I. Pulsatory Andesite Lava Flow at Bagana Volcano. *Geochemistry, Geophys. Geosystems*. **2012**, *13* (11), 11. <https://doi.org/10.1029/2012GC004336>.
- Wadge, G.; McCormick Kilbride, B. T.; Edmonds, M.; Johnson, R. W. Persistent Growth of a Young Andesite Lava Cone: Bagana Volcano, Papua New Guinea. *J. Volcanol. Geotherm. Res.* **2018**, *356*, 304–315. <https://doi.org/10.1016/j.jvolgeores.2018.03.012>.
- Walter, T. R.; Subandriyo, J.; Kirbani, S.; Bathke, H.; Suryanto, W.; Aisyah, N.; Darmawan, H.; Jousset, P.; Luehr, B. G.; Dahm, T. Volcano-Tectonic Control of Merapi's Lava Dome Splitting: The November 2013 Fracture Observed from High Resolution TerraSAR-X Data. *Tectonophysics*. **2015**, *639*, 23–33. <https://doi.org/10.1016/j.tecto.2014.11.007>.
- Wantim, M. N.; Suh, C. E.; Ernst, G. G. J.; Kervyn, M.; Jacobs, P. Characteristics of the 2000 Fissure Eruption and Lava Flow Fields at Mount Cameroon Volcano, West Africa: A Combined Field Mapping and Remote Sensing Approach. *Geol. J.* **2011**, *46* (4), 344–363. <https://doi.org/10.1002/gj.1277>.
- Wantim, M. N.; Kervyn, M.; Ernst, G. G. J.; del Marmol, M. A.; Suh, C. E.; Jacobs, P. Numerical Experiments on the Dynamics of Channelised Lava Flows at Mount Cameroon Volcano with the FLOWGO Thermo-Rheological Model. *J. Volcanol. Geotherm. Res.* **2013**, *253*, 35–53. <https://doi.org/10.1016/j.jvolgeores.2012.12.003>.
- Watanabe, H.; Matsuo, K. Rock Type Classification by Multi-Band TIR of ASTER. *Geosci. J.* **2003**, *7* (4), 347–358. <https://doi.org/10.1007/bf02919567>.
- Watt, S. F. L.; Pyle, D. M.; Mather, T. A. Evidence of Mid- to Late-Holocene Explosive Rhyolitic Eruptions from Chaitén Volcano, Chile. *Andean Geol.* **2013**, *40* (2), 216–226. <https://doi.org/10.5027/andgeov40n2-a02>.
- Wessels, R. L.; Coombs, M. L.; Schneider, D. J.; Dehn, J.; Ramsey, M. S. High-Resolution Satellite and Airborne Thermal Infrared Imaging of the 2006 Eruption of Augustine Volcano. *US Geol. Surv. Prof. Pap.* **2010**, *1769* (1769), 527–552. <https://doi.org/10.3133/pp176922>.
- Wessels, R. L.; Vaughan, R. G.; Patrick, M. R.; Coombs, M. L. High-Resolution Satellite and Airborne Thermal Infrared Imaging of Precursory Unrest and 2009 Eruption at Redoubt Volcano, Alaska. *J. Volcanol. Geotherm. Res.* **2013**, *259*, 248–269. <https://doi.org/10.1016/j.jvolgeores.2012.04.014>.
- West, M. E. Recent Eruptions at Bezymianny Volcano—A Seismological Comparison. *J. Volcanol. Geotherm. Res.* **2013**, *263*, 42–57. <https://doi.org/10.1016/j.jvolgeores.2012.12.015>.
- Whelley, P. L.; Newhall, C. G.; Bradley, K. E. The Frequency of Explosive Volcanic Eruptions in Southeast Asia. *Bull. Volcanol.* **2015**, *77* (1), 1. <https://doi.org/10.1007/s00445-014-0893-8>.
- Williams, D. B.; Ramsey, M. S. On the Applicability of Laboratory Thermal Infrared Emissivity Spectra for Deconvolving Satellite Data of Opaque Volcanic Ash Plumes. *Remote Sens.* **2019**, *11* (19), 2318. <https://doi.org/10.3390/rs11192318>.
- Williams, D. B.; Ramsey, M. S.; Wickens, D. J.; Karimi, B. Identifying Eruptive Sources of Drifting Volcanic Ash Clouds Using Back-Trajectory Modeling of Spaceborne Thermal Infrared Data. *Bull. Volcanol.* **2019**, *81* (9), 53. <https://doi.org/10.1007/s00445-019-1312-y>.
- Worden, A.; Dehn, J.; Ripepe, M.; Donne, D. D. Frequency Based Detection and Monitoring of Small Scale Explosive Activity by Comparing Satellite and Ground Based Infrared Observations at Stromboli Volcano, Italy. *J. Volcanol. Geotherm. Res.* **2014**, *283*, 159–171. <https://doi.org/10.1016/j.jvolgeores.2014.07.007>.
- Worni, R.; Huggel, C.; Stoffel, M.; Pulgarín, B. Challenges of Modeling Current Very Large Lahars at Nevado Del Huila Volcano, Colombia. *Bull. Volcanol.* **2012**, *74* (2), 309–324. <https://doi.org/10.1007/s00445-011-0522-8>.
- Wright, R.; Rothery, D. A.; Blake, S.; Harris, A. J. L.; Pieri, D. C. Simulating the Response of the EOS Terra ASTER Sensor to High-Temperature Volcanic Targets. *Geophys. Res. Lett.* **1999**, *26* (12), 1773–1776. <https://doi.org/10.1029/1999GL900360>.

- Wright, R.; Rothery, D. A.; Blake, S.; Pieri, D. C. Improved Remote Sensing Estimates of Lava Flow Cooling: A Case Study of the 1991–1993 Mount Etna Eruption. *J. Geophys. Res. Solid Earth*. **2000**, *105* (B10), 23681–23694. <https://doi.org/10.1029/2000jb900225>.
- Wright, R.; Carn, S. A.; Flynn, L. P. A Satellite Chronology of the May–June 2003 Eruption of Anatahan Volcano. *J. Volcanol. Geotherm. Res.* **2005**, *146* (1–3 SPEC. ISS.), 102–116. <https://doi.org/10.1016/j.jvolgeores.2004.10.021>.
- Wright, R.; Garbeil, H.; Davies, A. G. Cooling Rate of Some Active Lavas Determined Using an Orbital Imaging Spectrometer. *J. Geophys. Res. Solid Earth*. **2010**, *115* (6). <https://doi.org/10.1029/2009JB006536>.
- Xi, X.; Johnson, M. S.; Jeong, S.; Fladeland, M.; Pieri, D.; Diaz, J. A.; Bland, G. L. Constraining the Sulfur Dioxide Degassing Flux from Turrialba Volcano, Costa Rica Using Unmanned Aerial System Measurements. *J. Volcanol. Geotherm. Res.* **2016**, *325*, 110–118. <https://doi.org/10.1016/j.jvolgeores.2016.06.023>.
- Yamaguchi, Y.; Kahle, A. B.; Tsu, H.; Kawakami, T.; Pniel, M. Overview of Advanced Spaceborne Thermal Emission and Reflection Radiometer (ASTER). *IEEE Trans. Geosci. Remote Sens.* **1998**, *36* (4), 1062–1071. <https://doi.org/10.1109/36.700991>.
- Yulianto, F.; Suwarsono; Sofan, P. The Utilization of Remotely Sensed Data to Analyze the Estimated Volume of Pyroclastic Deposits and Morphological Changes Caused by the 2010–2015 Eruption of Sinabung Volcano, North Sumatra, Indonesia. *Pure Appl. Geophys.* **2016**, *173* (8), 2711–2725. <https://doi.org/10.1007/s00024-016-1342-8>.
- Zlotnicki, J.; Sasai, Y.; Toutain, J. P.; Villacorte, E. U.; Bernard, A.; Sabit, J. P.; Gordon, J. M.; Corpuz, E. G.; Harada, M.; Punongbayan, J. T.; et al. Combined Electromagnetic, Geochemical and Thermal Surveys of Taal Volcano (Philippines) during the Period 2005–2006. *Bull. Volcanol.* **2009**, *71* (1), 29–47. <https://doi.org/10.1007/s00445-008-0205-2>.
- Zouzias, D.; Miliareisis, G. C.; Seymour, K. S. Interpretation of Nisyros Volcanic Terrain Using Land Surface Parameters Generated from the ASTER Global Digital Elevation Model. *J. Volcanol. Geotherm. Res.* **2011**, *200* (3–4), 159–170. <https://doi.org/10.1016/j.jvolgeores.2010.12.012>.

References

- Kahle, A.B.; Palluconi, F.D.; Hook, S.J.; Realmuto, V.J.; Bothwell, G. The Advanced Spaceborne Thermal Emission and Reflectance Radiometer (Aster). *Int. J. Imaging Syst. Technol.* **1991**, *3*, 144–156. [[CrossRef](#)]
- Ramsey, M.S. Synergistic Use of Satellite Thermal Detection and Science: A Decadal Perspective Using ASTER. *Geol. Soc. Spec. Publ.* **2016**, *426*, 115–136. [[CrossRef](#)]
- Pieri, D.; Abrams, M. ASTER Watches the World’s Volcanoes: A New Paradigm for Volcanological Observations from Orbit. *J. Volcanol. Geotherm. Res.* **2004**, *135*, 13–28. [[CrossRef](#)]
- Urai, M. Sulfur Dioxide Flux Estimation from Volcanoes Using Advanced Spaceborne Thermal Emission and Reflection Radiometer—A Case Study of Miyakejima Volcano, Japan. *J. Volcanol. Geotherm. Res.* **2004**, *134*, 1–13. [[CrossRef](#)]
- Carter, A.; Ramsey, M. Long-Term Volcanic Activity at Shiveluch Volcano: Nine Years of ASTER Spaceborne Thermal Infrared Observations. *Remote Sens.* **2010**, *2*, 2571–2583. [[CrossRef](#)]
- Ramsey, M.S.; Wessels, R.L.; Anderson, S.W. Surface Textures and Dynamics of the 2005 Lava Dome at Shiveluch Volcano, Kamchatka. *Bull. Geol. Soc. Am.* **2012**, *124*, 678–689. [[CrossRef](#)]
- Yamaguchi, Y.; Kahle, A.B.; Tsu, H.; Kawakami, T.; Pniel, M. Overview of Advanced Spaceborne Thermal Emission and Reflection Radiometer (ASTER). *IEEE Trans. Geosci. Remote Sens.* **1998**, *36*, 1062–1071. [[CrossRef](#)]
- Gillespie, A.; Rokugawa, S.; Matsunaga, T.; Cothorn, J.S.; Hook, S.; Kahle, A.B. A temperature and emissivity separation algorithm for Advanced Spaceborne Thermal Emission and Reflection Radiometer (ASTER) images. *IEEE Trans. Geosci. Remote Sens.* **1998**, *36*, 1113–1126. [[CrossRef](#)]
- Hirano, A.; Welch, R.; Lang, H. Mapping from ASTER Stereo Image Data: DEM Validation and Accuracy Assessment. *ISPRS J. Photogramm. Remote Sens.* **2003**, *57*, 356–370. [[CrossRef](#)]

10. ASTER Validation Team (AVT). *ASTER Global DEM Validation Summary Report*; report no. 28; The Ministry of Economy, Trade and Industry (METI) and the National Aeronautics and Space Administration (NASA): Washington, DC, USA, 2009.
11. Tachikawa, T.; Hato, M.; Kaku, M.; Iwasaki, A. Characteristics of ASTER GDEM version 2. In *Proceedings of the 2011 IEEE International Geoscience and Remote Sensing Symposium*, Vancouver, BC, Canada, 24–29 July 2011; pp. 3657–3660.
12. National Research Council (NRC). *Thriving on Our Changing Planet: A Decadal Strategy for Earth Observation from Space*; The Natl. Acad. Press: Washington, DC, USA, 2018; 560p, ISBN 978-0-309-46757-5.
13. Gawarecki, S.J.; Lyon, R.J.P.; Nordberg, W. Infrared spectral returns and imagery of the Earth from space and their application to geological problems: Scientific experiments for manned orbital flight. *Am. Astronaut. Soc. Sci. Technol.* **1965**, *4*, 13–133.
14. Williams, R.S., Jr.; Friedman, J.D. Satellite Observation of Effusive Volcanism. *Br. Interplanet. Soc. J.* **1970**, *23*, 441–450.
15. Scorer, R.S. Etna: The Eruption of Christmas 1985 As Seen By Meteorological Satellite. *Weather* **1986**, *41*, 378–384. [[CrossRef](#)]
16. Harris, A. *Thermal Remote Sensing of Active Volcanoes: A User's Manual*; Cambridge University Press: Cambridge, UK, 2013.
17. Ramsey, M.S.; Harris, A.J.L. Volcanology 2020: How Will Thermal Remote Sensing of Volcanic Surface Activity Evolve over the next Decade? *J. Volcanol. Geotherm. Res.* **2013**, *249*, 217–233. [[CrossRef](#)]
18. Harris, A.J.L.; Butterworth, A.L.; Carlton, R.W.; Downey, I.; Miller, P.; Navarro, P.; Rothery, D.A. Low-Cost Volcano Surveillance from Space: Case Studies from Etna, Krafla, Cerro Negro, Fogo, Lascar and Erebus. *Bull. Volcanol.* **1997**, *59*, 49–64. [[CrossRef](#)]
19. Wright, R.; Flynn, L.; Garbeil, H.; Harris, A.; Pilger, E. Automated Volcanic Eruption Detection Using MODIS. *Remote Sens. Environ.* **2002**, *82*, 135–155. [[CrossRef](#)]
20. Hirn, B.R.; Di Bartola, C.; Laneve, G.; Cadau, E.; Ferrucci, F. SEVIRI onboard Meteosat Second Generation, and the quantitative monitoring of effusive volcanoes in Europe and Africa. In *Proceedings of the IEEE International Geoscience and Remote Sensing Symposium (IGARSS 2008)*, Boston, MA, USA, 7–11 July 2008; Inst. of Electr. and Electron. Eng.: New York, NY, USA, 2008; pp. 374–377.
21. Ramsey, M.S.; Chevrel, M.O.; Coppola, D.; Harris, A.J.L. The Influence of Emissivity on the Thermo-Rheologic AI Modeling of the Channelized Lava Flows at Tolbachik Volcano. *Ann. Geophys.* **2019**, *61*. [[CrossRef](#)]
22. Reath, K.A.; Ramsey, M.S.; Dehn, J.; Webley, P.W. Predicting Eruptions from Precursory Activity Using Remote Sensing Data Hybridization. *J. Volcanol. Geotherm. Res.* **2016**, *321*, 18–30. [[CrossRef](#)]
23. National Research Council (NRC). *Earth Science and Applications from Space: National Imperatives for the Next Decade and Beyond*; The Natl. Acad. Press: Washington, DC, USA, 2007; 454p, ISBN 978-0-309-10387-9.
24. Raup, B.; Racoviteanu, A.; Khalsa, S.J.S.; Helm, C.; Armstrong, R.; Arnaud, Y. The GLIMS Geospatial Glacier Database: A New Tool for Studying Glacier Change. *Glob. Planet. Chang.* **2007**, *56*, 101–110. [[CrossRef](#)]
25. Ramsey, M.S. Mapping the City Landscape from Space: The Advanced Spaceborne Thermal Emission and Reflectance Radiometer (ASTER) Urban Environmental Monitoring Program. *Earth Sci. City* **2003**, *1*, 337–361. [[CrossRef](#)]
26. Urai, M.; Fukui, K.; Yamaguchi, Y.; Pieri, D. Volcano Observation Potential and Global Volcano Monitoring Plan with ASTER. *Bull. Volcanol. Soc. Japan* **1999**, *44*, 131–141. [[CrossRef](#)]
27. Urai, M.; Pieri, D. ASTER Applications in Volcanology. In *Remote Sensing and Digital Image Processing*; Ramachandran, B., Justice, C., Abrams, M., Eds.; NASA's Earth Observing System and the Science of ASTER and MODIS; Land Remote Sensing and Global Environmental Change; Springer: New York, NY, USA, 2011; Volume 11, pp. 245–272. [[CrossRef](#)]
28. Abrams, M.; Tsu, H.; Hulley, G.; Iwao, K.; Pieri, D.; Cudahy, T.; Kargel, J. The Advanced Spaceborne Thermal Emission and Reflection Radiometer (ASTER) after Fifteen Years: Review of Global Products. *Int. J. Appl. Earth Obs. Geoinf.* **2015**, *38*, 292–301. [[CrossRef](#)]
29. Duba, K.; Ramsey, M.; Wessels, R.; Dehn, J. Optical Satellite Volcano Monitoring: A Multi-Sensor Rapid Response System. *Geosci. Remote Sens.* **2009**, 473–496. [[CrossRef](#)]
30. Davies, A.G.; Chien, S.; Wright, R.; Miklius, A.; Kyle, P.R.; Welsh, M.; Johnson, J.B.; Tran, D.; Schaffer, S.R.; Sherwood, R. Sensor Web Enables Rapid Response to Volcanic Activity. *Eos (Wash. DC)* **2006**, *87*, 2–4. [[CrossRef](#)]

31. Wright, R.; Flynn, L.P.; Garbeil, H.; Harris, A.J.L.; Pilger, E. MODVOLC: Near-Real-Time Thermal Monitoring of Global Volcanism. *J. Volcanol. Geotherm. Res.* **2004**, *135*, 29–49. [[CrossRef](#)]
32. Coppola, D.; Laiolo, M.; Cigolini, C.; Donne, D.D.; Ripepe, M. Enhanced Volcanic Hot-Spot Detection Using MODIS IR Data: Results from the MIROVA System. *Geol. Soc. Lond. Spec. Publ.* **2016**, *426*, 181–205. [[CrossRef](#)]
33. Dehn, J.; Dean, K.; Engle, K. Thermal Monitoring of North Pacific Volcanoes from Space. *Geology* **2000**, *28*, 755–758. [[CrossRef](#)]
34. Urai, M. Volcano Observations with ASTER and ASTER Image Database for Volcanoes. *Int. Geosci. Remote Sens. Symp.* **2011**, *2011*, 3661–3663. [[CrossRef](#)]
35. Amici, S.; Piscini, A.; Buongiorno, M.F.; Pieri, D. Geological Classification of Volcano Teide by Hyperspectral and Multispectral Satellite Data. *Int. J. Remote Sens.* **2013**, *34*, 3356–3375. [[CrossRef](#)]
36. Ramsey, M.S.; Flynn, L.P. Strategies, Insights, and the Recent Advances in Volcanic Monitoring and Mapping with Data from NASA’s Earth Observing System. *J. Volcanol. Geotherm. Res.* **2004**, *135*, 1–11. [[CrossRef](#)]
37. Scheidt, S.; Lancaster, N.; Ramsey, M.S. Eolian Dynamics and Sediment Mixing in the Gran Desierto, Mexico, Determined from Thermal Infrared Spectroscopy and Remote-Sensing Data. *Bull. Geol. Soc. Am.* **2011**, *123*, 1628–1644. [[CrossRef](#)]
38. Rose, S.R.; Watson, I.M.; Ramsey, M.S.; Hughes, C.G. Thermal Deconvolution: Accurate Retrieval of Multispectral Infrared Emissivity from Thermally-Mixed Volcanic Surfaces. *Remote Sens. Environ.* **2014**, *140*, 690–703. [[CrossRef](#)]
39. Flynn, I.T.W.; Ramsey, M.S. Uncertainties in Pyroclastic Density Current Hazard Assessments of Fuego Volcano, Guatemala. *Remote Sens.* **2020**, in review.
40. Henney, L.A.; Rodríguez, L.A.; Watson, I.M. A Comparison of SO₂ Retrieval Techniques Using Mini-UV Spectrometers and ASTER Imagery at Lascar Volcano, Chile. *Bull. Volcanol.* **2012**, *74*, 589–594. [[CrossRef](#)]
41. Realmuto, V.J. The potential use of the earth observing system data to monitor the passive emissions of sulfur dioxide from volcanoes. In *Remote Sensing of Active Volcanism, Geophysical Monograph 116*; AGU: Washington, DC, USA, 2000; pp. 101–115.
42. Patrick, M.R.; Witzke, C.-N. Thermal Mapping of Hawaiian Volcanoes with ASTER Satellite Data. *US Geol. Surv. Sci. Investig. Rep.* **2011**, *5110*, 22.
43. Rose, S.R.; Ramsey, M.S. The 2005 and 2007 Eruptions of Klyuchevskoy Volcano, Russia: Behavior and Effusion Mechanisms. In *Monitoring Volcanoes in the North Pacific: Observations from Space*; Dean, K.G., Dehn, J., Dehn, J., Eds.; -540-24125-6, 389 pp: DVD; Springer-Praxis Books: New York, NY, USA, 2015; pp. 973–978.
44. Harris, A.; Chevrel, M.; Coppola, D.; Ramsey, M.; Hrysiwicz, A.; Thivet, S.; Villeneuve, N.; Favalli, M.; Peltier, A.; Kowalski, P.; et al. Validation of an Integrated Satellite-Data-Driven Response to an Effusive Crisis: The April–May 2018 Eruption of Piton de La Fournaise. *Ann. Geophys. Geophys.* **2019**, *61*. [[CrossRef](#)]
45. Stevens, N.F.; Garbeil, H.; Mouginiis-Mark, P.J. NASA EOS Terra ASTER: Volcanic Topographic Mapping and Capability. *Remote Sens. Environ.* **2004**, *90*, 405–414. [[CrossRef](#)]
46. Huggel, C.; Schneider, D.; Miranda, P.J.; Delgado Granados, H.; Käab, A. Evaluation of ASTER and SRTM DEM Data for Lahar Modeling: A Case Study on Lahars from Popocatepetl Volcano, Mexico. *J. Volcanol. Geotherm. Res.* **2008**, *170*, 99–110. [[CrossRef](#)]
47. Ramsey, M.; Dehn, J. Spaceborne Observations of the 2000 Bezymianny, Kamchatka Eruption: The Integration of High-Resolution ASTER Data into near Real-Time Monitoring Using AVHRR. *J. Volcanol. Geotherm. Res.* **2004**, *135*, 127–146. [[CrossRef](#)]
48. Tralli, D.M.; Blom, R.G.; Zlotnicki, V.; Donnellan, A.; Evans, D.L. Satellite Remote Sensing of Earthquake, Volcano, Flood, Landslide and Coastal Inundation Hazards. *ISPRS J. Photogramm. Remote Sens.* **2005**, *59*, 185–198. [[CrossRef](#)]

